

RESEARCH ARTICLE

10.1002/2017TC004657

Key Points:

- Post Last Glacial Maximum tectonic activity along the Almaty range front is expressed in fault scarps in alluvial fans, folding, uplifted abandoned river terraces, and backthrusts
- Active deformation is laterally distributed, affecting the range front, the interior of the mountains, and the foreland
- The Holocene slip rate of the range front fault is $\sim 1.2\text{--}2.2$ mm/a in the eastern section

Supporting Information:

- Supporting Information S1

Correspondence to:

C. Grützner,
christoph.gruetzner@uni-jena.de

Citation:

Grützner, C., Walker, R. T., Abdрахmatov, K. E., Mukambaev, A., Elliott, A. J., & Elliott, J. R. (2017). Active tectonics around Almaty and along the Zailisky Alatau range front. *Tectonics*, 36, 2192–2226. <https://doi.org/10.1002/2017TC004657>



Received 11 MAY 2017

Accepted 20 SEP 2017

Accepted article online 11 OCT 2017

Published online 25 OCT 2017

Active Tectonics Around Almaty and along the Zailisky Alatau Range front

C. Grützner^{1,2} , R. T. Walker³, K. E. Abdрахmatov⁴, A. Mukambaev⁵, A. J. Elliott³ , and J. R. Elliott⁶
¹COMET, Bullard Laboratories, Cambridge University, Cambridge, UK, ²Now at Institute of Geological Sciences, Friedrich Schiller University Jena, Jena, Germany, ³COMET, Department of Earth Sciences, Oxford University, Oxford, UK, ⁴Institute of Seismology, National Academy of Sciences, Kyrgyz Republic, ⁵Data Center of the Institute of Geophysical Researches, Almaty, Kazakhstan, ⁶COMET, School of Earth and Environment, University of Leeds, Leeds, UK

Abstract The Zailisky Alatau is a >250 km long mountain range in Southern Kazakhstan. Its northern range front around the major city of Almaty has more than 4 km topographic relief, yet in contrast to other large mountain fronts in the Tien Shan, little is known about its Late Quaternary tectonic activity despite several destructive earthquakes in the historical record. We analyze the tectonic geomorphology of the range front fault using field observations, differential GPS measurements of fault scarps, historical and recent satellite imagery, meter-scale topography derived from stereo satellite images, and decimeter-scale elevation models from unmanned aerial vehicle surveys. Fault scarps ranging in height from ~ 2 m to >20 m in alluvial fans indicate that surface rupturing earthquakes occurred along the range front fault since the Last Glacial Maximum. Minimum estimated magnitudes for those earthquakes are $M_{6.8-7}$. Radiocarbon dating results from charcoal layers in uplifted river terraces indicate a Holocene slip rate of $\sim 1.2\text{--}2.2$ mm/a. We find additional evidence for active tectonic deformation all along the Almaty range front, basinward in the Kazakh platform, and in the interior of the Zailisky mountain range. Our data indicate that the seismic hazard faced by Almaty comes from a variety of sources, and we emphasize the problems related to urban growth into the loess-covered foothills and secondary earthquake effects. With our structural and geochronologic framework, we present a schematic evolution of the Almaty range front that may be applicable to similar settings of tectonic shortening in the mountain ranges of Central Asia.

1. Introduction

Almaty, the former capital of Kazakhstan and today expanding as the home to more than 1.7 million people, lies at the foothills of the Zailisky Alatau (Alatau: “colored mountains” in Kyrgyz). These mountains separate Lake Issyk-Kul in the south from the Kazakh platform to the north and form the northernmost range of the Tien Shan at this longitude (Figure 1a). Although being rather young—modern Almaty was founded as Verny in the 19th Century as a Russian garrison—the city has suffered from several strong and destructive earthquakes (Figure 1b). In 1887, the Verny earthquake with a magnitude of about 7.3 had its epicenter a few kilometers west of the city. The precise location is unknown since the earthquake occurred in the pre-instrumental era and no surface ruptures were reported (Tatevossian, 2007). The earthquake triggered numerous landslides (Mushketov, 1890) and led to several hundred fatalities (Hay, 1888). Only 2 years later, in 1889, the Chilik earthquake, with a magnitude of ~ 8 , ruptured the surface 100 km to the southeast of Almaty and led to severe shaking in the city (Abdрахmatov et al., 2016; Krüger et al., 2015). This earthquake produced ~ 175 km of surface ruptures and up to 10 m of surface slip (Abdрахmatov et al., 2016; Figure 1b). Finally, Almaty was heavily damaged by the 1911 Chon Kemin earthquake, with a magnitude of ~ 8 , which occurred on the southern flank of the Zailisky Alatau (Arrowsmith et al., 2017; Delvaux et al., 2001; Kulikova & Krüger, 2015). Up to ~ 200 km of surface ruptures and more than 10 m of slip resulted from this event (Arrowsmith et al., 2017; Figure 1b). Kondorskaya and Shebalin (1977) list a destructive earthquake that happened in 1807 with a magnitude of ~ 6.7 and cited Gorshkov (1947) and Mushketov and Orlov (1893) for this event. The epicenter is said to be beneath Almaty, and they report “Terrible catastrophe in Almata,” but no further information is available.

Fault scarps with cumulative heights of 50 m and higher are abundant along the Almaty range front as a result of the Quaternary shortening and uplift. However, apart from one scarp mapped by Tibaldi et al. (1997) near Almaty, no Holocene fault scarps, surface ruptures, recent deformation features, or other indicators for recent strong earthquakes have been documented along the northern Zailisky Alatau in the international literature.

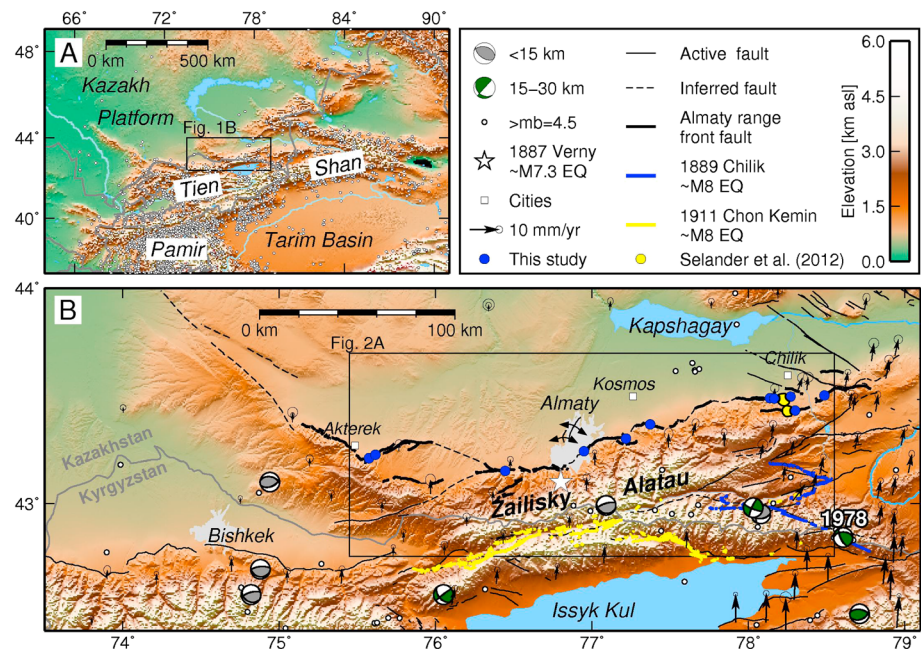


Figure 1. Tectonic setting in Central Asia of our study area of the Zailisky Alatau within the Tien Shan. (a) Instrumental seismicity is focused within the Pamir and around the margins of the Tarim Basin. (b) The Almaty range front fault marks the northern boundary of the Zailisky Alatau (black line). Blue dots denote the sites discussed in detail in this paper, and yellow dots show the location of the slip rate estimate of Selander et al. (2012). Beachballs show depth-colored earthquakes with focal mechanisms from body waveform modeling of Sloan et al. (2011). The location of the 1978 Dzhalanash–Tyup earthquake is marked (location from Krüger et al., 2015, and focal data from CMT, 2016). White dots are earthquakes $m_b > 4.5$ from the catalog of Engdahl et al. (1998) and updates thereof from 1960 to 2008 and the ISC catalog (ISC, 2016) from 2009 to 2016. Blue lines are the surface ruptures of the 1889 M_W 8.0–8.3 Chilik earthquake (Bindi et al., 2014; Krüger et al., 2015; Abdrakhmatov et al., 2016; own mapping). Yellow lines are the surface ruptures of the M_W ~8.0 1911 Chon Kemin earthquake (Arrowsmith et al., 2017; Bogdanovich et al., 1914; Crosby et al., 2007). The epicenter of the 1887 Verny $M7.3$ earthquake is from Kondorskaya and Shebalin (1977) and fits macroseismic data from Mushketov (1890) as discussed in Tatevossian (2007). GPS velocities relative to stable Eurasia are shown with 95% confidence ellipses (Zubovich et al., 2010). Note the anticline in the northern outskirts of Almaty indicated by double-head arrows. Topography is from SRTM1 data.

Also, with the exception of the easternmost section of the range near Chilik (Selander et al., 2012), no slip rate of the range front fault has been published.

The geographical setting of Almaty is somewhat similar to that of Bishkek, the capital of neighboring Kyrgyzstan, with both positioned at the foot of subranges of the northern Tien Shan (Figure 1b) mountain front. Bishkek, however, is located on the footwall of a thrust fault that uplifted Neogene units in the Quaternary to an intermediate elevation between the high ranges and the foreland. Abundant evidence for Holocene faulting can be found there. Fault scarps that offset alluvial fans by ≥ 2 m are present, and paleoseismological trenches across the frontal Issyk-Ata Fault reveal evidence of at least two surface-rupturing earthquakes in the past ~10,000 years (Landgraf et al., 2016). Thompson (2001) reports four surface-rupturing events since the Last Glacial Maximum (LGM) from the range front, and Smekalin et al. (2016) identified an earthquake that happened ~3,000 B.P. These findings illustrate that Bishkek, with its ~850,000 inhabitants, is built along an active fault that has ruptured in earthquakes of $M > 7$ in the past and will do so again in the future. Although Bishkek can suffer from the far-field effects of distant $M \sim 8$ earthquakes like the 1889 Chilik and 1911 Chon Kemin events, smaller local events may have the potential to be even more devastating due to the elevated proximal ground motion in the near field.

Given the along-strike evidence of faulting and the overall shortening across the region, the absence of published mapped evidence for Holocene activity on the range front adjacent to Almaty is curious, as the 250 km long, minimally embayed range has impressive relief with up to 5,000 m high mountains overlooking the <900 m Kazakh platform. There is clear evidence that vertical tectonic motion has been localized here since the uplift of this part of the Tien Shan in the Neogene (Abdrakhmatov et al., 2016; Avouac et al., 1993). We

investigate three possibilities to explain the previous absence of recorded activity: (i) The range front is indeed seismically inactive, and during or before the Holocene, deformation migrated elsewhere. Earthquakes like the 1887 Verny event occur on faults in the higher parts of the Zailisky Alatau where traces of active faulting are subject to fast erosion and/or difficult to identify, or they occur buried within the Kazakh platform without clear surface expression. (ii) The range front is seismically active, but the recurrence intervals of large events are so long that any morphological evidence has been obliterated by erosion and sedimentation. (iii) The range front is seismically active, and geomorphological evidence for past surface-rupturing earthquakes does exist but has been overlooked thus far.

In this paper we review all available evidence for active faulting along the Zailisky Alatau. The geomorphological evidence for active tectonics is investigated at 11 different sites (labeled S1–S11 from west to east) along the northern front of the Zailisky Alatau. We cover a ~250 km long section of the range front centered on Almaty (Figure 2a) using field observations, remote sensing, and dating of Late Quaternary deformation. We document clear evidence for surface rupturing earthquakes since the LGM and provide the first estimate of a slip rate on the fault based on Quaternary dating of measured offsets. Finally, we put our morphologic observations of the Almaty range front into the wider regional context to explore implications for the tectonic evolution and seismic hazard of the Tien Shan.

2. Methods

We applied a wide set of methods to detect and document morphological evidence of active tectonics, including remote sensing, photogrammetric techniques, differential GPS profiles, field mapping, and Quaternary dating.

2.1. Satellite Imagery and Digital Elevation Models

SRTM1 elevation data and the ALOS JAXA digital elevation model (DEM) were used to produce slope, hillshade, aspect, and terrain ruggedness index (TRI) maps of the Zailisky Alatau with QGIS (QGIS Development Team, 2017). The TRI is a measure for the difference in elevation between a raster cell and its neighboring cells (Riley et al., 1999). It reveals landscape features characterized by changes in slope and with high relief, such as areas of uplift by faulting or river incision. These data allow us to observe large-scale features of tectonic geomorphology over wide areas as they have a ground resolution of 30×30 m. To overcome the issue of the relatively low resolution of these global data sets, we acquired SPOT6 stereo satellite imagery of a narrow strip along parts of the range front. This data set has a ground resolution of 1.5 m, and we produced a DEM with 3 m ground resolution using commercial software (ERDAS IMAGINE).

Optical satellite images were used to identify fault scarps and lineaments. We analyzed recent and past Google Earth imagery (1984–2017; DigitalGlobe–Landsat/Copernicus, Cnes/SPOT), the SPOT6 data, and declassified Corona satellite imagery (~2 m resolution) from the 1960s. The latter has the advantage of covering a time at which some tectonic features were not yet obliterated by urban development and infrastructure projects (Mackenzie et al., 2016).

2.2. Field-Based Drone DEMs

We produced high-resolution DEMs from aerial images collected from an unmanned aerial vehicle (drone) to analyze the geomorphological setting of several sites in detail. A DJI Phantom 2 quad-copter was used to carry a Canon PowerShot SX230 HS compact camera with internal GPS receiver to take hundreds of overlapping images from up to 50 m altitude. Commercial software (AgiSoft Photoscan) was used to produce a point cloud and a DEM with the Structure-from-Motion method (e.g., Bemis et al., 2014). Ground control points for reference were located with differential GPS (DGPS). Further details of our survey and processing steps are reported in Abdrakhmatov et al. (2016). The resolution of the DEMs is on the order of 0.1 m, and they typically cover areas of $0.2\text{--}0.5\text{ km}^2$. As with the satellite data, we computed slope and hillshade maps to visualize the deformation features. The DEMs will be made available through OpenTopography (www.opentopography.org).

2.3. Offset Measurements at Scarps

We measured the vertical offsets of planar geomorphic markers such as alluvial fans and river terraces. Elevation profiles and swaths were extracted using QGIS algorithms. We used swath profiles for the

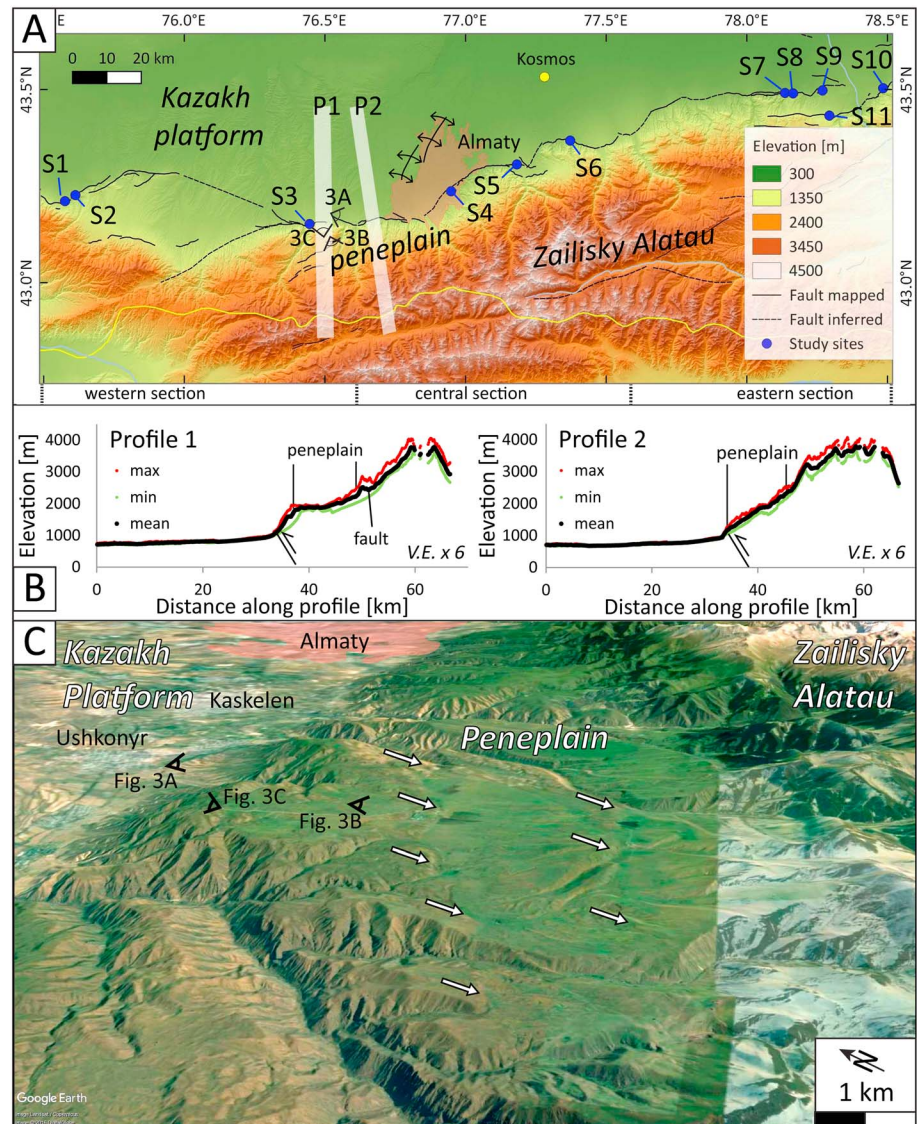


Figure 2. Morphology of our study area. (a) The 10 sites S1–S11 discussed in this paper (marked with blue dots) span the entire 250 km long Almaty range front. West of Almaty, anticlines strike NE (black double-headed arrows). The yellow dot marks the deformed sediments at the Kosmos site of Macklin et al. (2015). White rectangles mark the two topographic swath profiles in Figure 2b. Black symbols with capital letters mark the view direction of the photos in Figure 3. Pink shading denotes the outline extent of the urban development of Almaty. (b) Topographic swath profiles (vertically exaggerated 6X) illustrate the elevation difference between the Kazakhstan platform (<1,000 m) and the Zailiysky Alatau (up to 4,000 m). Note the smooth peneplain surface in both profiles and the topographic high at the fault described in section 3. (c) Oblique view looking east across the Kazakhstan platform, the peneplain, and the high Zailiysky Alatau. White arrows indicate south-facing fault scarps near Ushkonyr. Imagery: GoogleEarth.

SRTM1-based elevation data to show the larger-scale topography. The drone-DEMs and the SPOT6-DEM were analyzed using narrow single-track profiles in order to make use of the very high resolution. By fitting straight lines to the profile segments above and below the scarps, respectively, the vertical offset at the fault scarps was calculated using linear regression and the vertical separation between the two fitted lines at the steepest part of the scarp. In the case of surfaces that have the same dip both in the hanging wall and in the footwall of the fault, the along-profile location of the fault surface projection does not influence the measured vertical offsets. However, when the dips on either side of the fault do vary, the selection of fault location affects the result of the estimated offset based upon the elevation measurements. For most sites analyzed here, we do not know the exact location of the fault projection to the surface from outcrops. In these cases, the

position of the fault was defined at the location of the maximum slope angle of the scarp. Surveys of the present-day streambeds showed that the post-depositional tilt of the fitted surfaces is negligible. The geometrical error introduced by the landform geometry in the sense of Mackenzie and Elliott (2017) also does not affect our results significantly beyond the noted 10% uncertainties.

Uncertainty in the precise fault location is difficult to quantify without independent information, for example, from paleoseismological trenching or outcrop studies. Further errors stem from the vertical resolution of the DEMs and the nonplanar behavior of the upper and lower fan surfaces used to estimate the offset. The SRTM1 data have a vertical accuracy and resolution of a few meters (Smith & Sandwell, 2003), but it is impossible to quantify the relative accuracy of nearby point positions across the fault. We estimate the resolution of the SPOT DEM to be down to 3 m under favorable conditions but less than that in areas with steep slopes. The drone DEMs have an error of less than 0.5 m, which comes from the image quality, the photo matching process, and the uncertainty in the DGPS locations of the ground control points, which is <0.1 m. We expect the combined error of the vertical offsets measured for this study to be around 10%, but we assign at least ± 1 m error for each offset to factor in the uncertainties related to the geological setting, choice of profile location, etc. The purpose of this paper is mainly to document a variety of morphological evidence for active faulting along the Almaty range front. With the exception of one site, we do not measure slip rates for which a more in-depth calculation of the offset errors would be required. We thus report the measured offsets without the errors in the following, and we emphasize that we present first-order observations that allow us to draw a general picture of the regional tectonics.

At two of our sites, we used real-time kinematic DGPS profiles instead of elevation data extracted from the DEMs to measure the offset of river terraces. Thus, the error is reduced to the uncertainty of the DGPS measurements (<0.1 m) and the location of the fault along profile. Specific details of the measurements made at individual sites are described in the appropriate site description.

2.4. Radiocarbon Dating

Radiocarbon dating at site S7 was performed on charcoal and charcoal-bearing bulk sediment samples in silty layers. The samples were sent to BETA Analytic Inc. (Miami, FL, USA) for AMS radiocarbon dating. Standard acid/alkali/acid or acid wash pretreatment was applied to the samples, and INTCAL13 (Reimer et al., 2013) was used for calibration.

3. Geology, Tectonic Setting, and Geomorphology

3.1. Geological Background

The Tien Shan is an E–W trending mountain belt that has formed due to the collision of India and Eurasia in the Cenozoic. The mountain range is located more than 1,000 km north of the actual plate boundary delineated by the Himalaya, but GPS studies show that ~ 12 mm/a of the total N–S shortening is taken up in the eastern Tien Shan and ~ 20 mm/a in the western part—a sizeable portion of the overall India–Eurasia convergence (Abdrakhmatov et al., 1996; Zubovich et al., 2010). This E–W gradient in the rate of shortening is due to the clockwise rotation of the relatively rigid Tarim Basin, bounding the Tien Shan to the south, about a Euler pole located near the eastern end of the Tien Shan range (Avouac et al., 1993). GPS data also reveal a component of left-lateral shear in the area between Lake Issyk Kul and the stable Kazakh platform. Relatively large spacing and uncertainties in the GPS velocities of Zubovich et al. (2010) do not permit the discrimination of active faulting located precisely at the range front (England & Molnar, 2015).

Continental crustal growth took place by the accretion of a large subduction–accretion complex during the Paleozoic (Burtman, 1975; Windley et al., 1990). These rocks now form the basement of the Tien Shan. In the Mesozoic and the early Cenozoic, tectonic quiescence led to the creation of a vast erosional surface or peneplain (Burbank et al., 1999; Goryachev, 1959; Makarov, 1977). While the uplift of parts of the Tien Shan started before the Neogene, the latest phase of uplift in the Northern Tien Shan piedmonts has been ongoing since the Late Miocene (Bullen et al., 2003; Sobel et al., 2006). The erosional surface has been uplifted in the most recent phase of mountain growth and is preserved in many parts of the Tien Shan as a convenient marker for differential uplift (Oskin & Burbank, 2007; Sobel et al., 2006; Figure 3). The fact that the peneplain is so well preserved in many places indicates rather rapid uplift throughout the mountain range (Buslov et al., 2008). Uplift has occurred along \sim E–W trending thick-skinned reverse faults as evidenced by uplifted basement

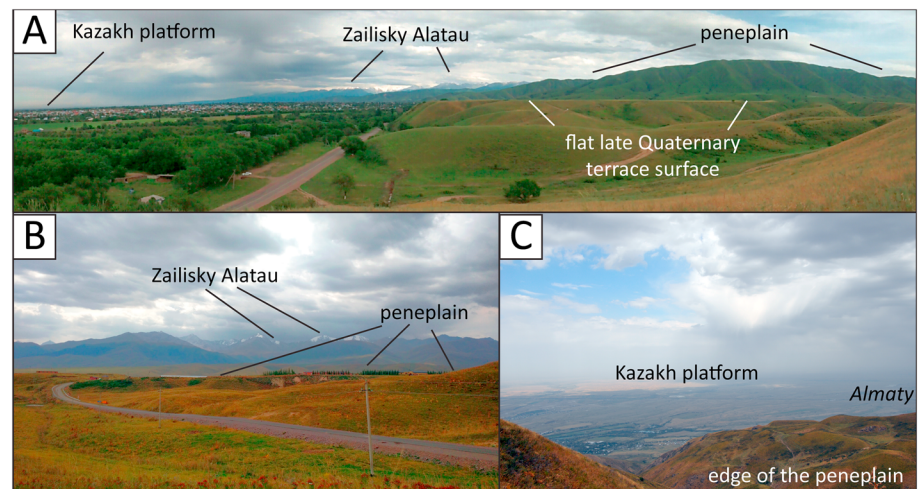


Figure 3. (a) View eastward from the platform to the high Zailisky Alatau (N 43.170602°, E 76.531304°). Flat Quaternary terraces surfaces covered in a layer of loess are uplifted in front of the Mesozoic erosional surface. (b) View southward from the peneplain toward the Zailisky Alatau (N 43.089242°, E 76.483833°). (c) View northward from the peneplain toward the Kazakh platform (N 43.124964°, E 76.473749°).

complexes (e.g., Abdrakhmatov et al., 2001). The basement along the range front mainly consist of Carboniferous–Permian series and granitic, granodioritic, and dioritic intrusives (Nalivkin, 1983).

North and south of the Tien Shan, flexural foreland basins contain up to several kilometers of sediment (see Avouac et al., 1993, and references therein). For example, the Kashi Basin in the Western Tarim is filled with 6–10 km of Neogene sediment (Sobel et al., 2006). The high ranges alternate with ~E–W elongated intermontane and intramontane basins filled with Cenozoic deposits as a result of increased erosion during mountain building. These basins record active tectonic deformation along the mountain fronts but also highlight deformation away from the ranges toward the basin centers in the form of folds and fault scarps in alluvial fan and fluvial terrace sequences (e.g., Abdrakhmatov et al., 2002; Brown et al., 1998; Thompson et al., 2002).

Glacial advances in the Tien Shan do not strictly coincide with the global LGM (Takeuchi et al., 2014; Zech, 2012). Glacial advances during the last glacial cycle were probably at their maximum around marine isotopic stage (MIS) 4 (~60–70 ka), but younger moraines are also preserved (Zech, 2012). For example, Koppes et al. (2008) report regional advances during MIS 3 and document locally preserved MIS 2 remains near modern glaciers. The sparse data set available makes it difficult to identify those glacial advances that left a major impact in the landscape in the form of alluvial fan series or river terraces. Therefore, we use the term LGM here in the sense of the global LGM around 26–19 ka (Clark et al., 2009). A regional correlation of river terraces has been established in the Tien Shan based on morphological arguments (Burgette et al., 2017; Thompson et al., 2002, and references therein). Four main terraces QI–QIV represent, respectively, early Pleistocene, middle Pleistocene, late Pleistocene, and Holocene stages of terrace formation and may again be subdivided into several substages. Although the local terrace systems may differ from the observed regional pattern, some main features seem to be characteristic for Tien Shan terraces in general. In the absence of Quaternary dating, those terraces may be used to estimate the approximate age of geomorphic markers.

3.2. Tectonic Setting and Seismicity

Instrumental seismicity in the Tien Shan is high compared to the forelands, with greater activity along its southern boundary and at the contact between the Tien Shan and the Pamir (Figure 1). Earthquakes in the Tien Shan typically have depths of 15–30 km. Deeper events are mainly recorded in the forelands. In the area of the Zailisky Alatau, only a few earthquakes for which moment tensor solutions could be determined from teleseismic waveform analyses occurred in the instrumental period (Sloan et al., 2011). These events have mostly reverse mechanisms, although some occurred on strike-slip faults. In general, instrumental earthquakes in the study area cannot be ascribed individual faults due to the lack of surface breaks and the

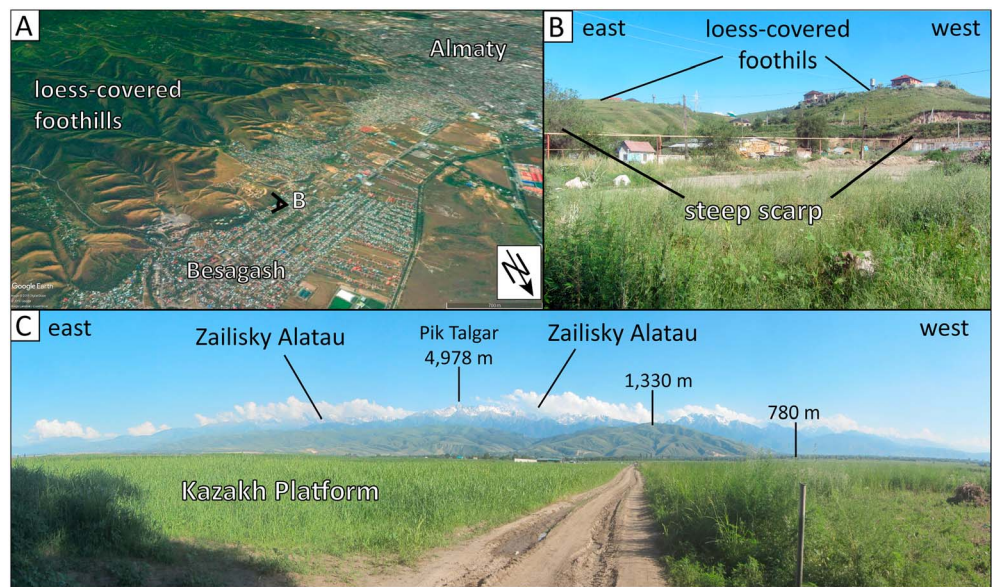


Figure 4. General geomorphic features of the Almaty range front. (a) The Almaty metropolitan area is growing along the range front, resulting in more people living directly above or close to the active faults. Urban development increasingly occupies the loess-covered foothills, for example, south of Besagash. B marks the position of photo in Figure 4b. Google Earth imagery. (b) View to the south toward the Almaty range front in Besagash. Note the steep scarp in front of the foothills and the new houses on top of the loess-covered hills. (c) Panorama view of the Zailisky Alatau at Talgar (77.3°E). Pik Talgar is the highest mountain in the mountain range. In front of the high Alatau, loess-covered hills reach up to ~1300 m. The Kazakh platform lies below 800 m.

abundance of possible seismogenic structures. Furthermore, the location errors are high compared to the spacing of mapped active faults. Moderate instrumental seismicity and microseismicity are well documented for Almaty and the surrounding regions (Mikhailova et al., 2015; Torizin et al., 2009). The historical record reaches back only a few hundred years but includes two of the strongest continental earthquakes on record. Both the 1889 Chilik and the 1911 Chon Kemin earthquake had magnitudes of $M \sim 8$ and produced significant surface ruptures. No surface ruptures were reported for the 1887 $M \sim 7.3$ Verny earthquake, and it remains unknown whether it occurred on the range front fault or in the mountains (Figure 1b). Paleoseismological data on earthquakes are available from the Issyk-Ata Fault south of Bishkek (Landgraf et al., 2016; Thompson, 2001), from the Toraigyr Fault east of Almaty (Grützner et al., 2017), and from the northern shores of Lake Issyk-Kul (e.g., Korjenkov et al., 2006, 2007, 2011). These data show that faults tend to break in large earthquakes but have recurrence intervals of several thousand years. These long intervals can lead to a near-complete obliteration of the surface expression of active faulting in between two successive events (Grützner et al., 2017). Another major issue for the preservation of fault scarps and other tectonic features is burial beneath the abundant loess cover in the piedmonts (Fitzsimmons et al., 2016).

A large number of active faults, especially in the Almaty area, are published on geological maps. Oscillating differential vertical motion in Almaty of up to 5 mm/a across faults was reported by Atrushkevitch et al. (1988) based on geodetic measurements made across a leveling network. The authors speculate on a relation with moderate to strong earthquakes that occurred up to 200 km away elsewhere in the Tien Shan, for which the observed vertical motion could serve as a precursor. However, no nearby strong earthquakes occurred in the observation period that could be tied to tectonic motion along those faults. Nontectonic causes like groundwater charge and discharge are known to produce differential motion along faults (e.g., Cuenca et al., 2013), and several other factors might lead to similar patterns of surface deformation. Tibaldi et al. (1997) report a 2–20 m high scarp east of Almaty and interpret it as the surface expression of a SW–NE striking fault-propagation fold. Unfortunately, this feature coincides with the terrace risers of the Small Almatinka River (Малая Алматинка), and thus, its usefulness as a geomorphic marker for fault activity may be compromised.

3.3. Morphology of the Zailisky Alatau Rangefront

The ENE trending Zailisky Alatau (Figures 1 and 2a) is the northernmost range of the Tien Shan between 75° and 78.5°E. It reaches an elevation of almost 5,000 m above sea level (Pik Talgar near Almaty; Figure 4). The Chon Kemin valley separates the Zailisky Alatau from the Kungey Range in the south. The Kazakh platform north of the Zailisky Alatau has an elevation of 900–1,000 m near the rangefront and gently decreases in elevation further north. The highest parts of the Zailisky Alatau have rather flat tops with deeply incised valleys in between them, indicating that the elevated Mesozoic peneplain still controls the morphology. Between the foreland and the highest peaks, pronounced north dipping surfaces with little relief mark the uplifted remnants of the Mesozoic peneplain (Figures 2–4). The morphology suggests that these intermediate-height peneplain surfaces are bounded by reverse faults on both sides.

Large parts of the rangefront are covered in thick loess deposits (Figure 4). Loess is found between ~750 and 2,400 m elevation, with the thickest deposits in the foothills of the Northern Tien Shan occurring around 1,000–1,300 m (Machalett et al., 2006). In the central part of the mountain range near Almaty (at Remisovka; Fitzsimmons et al., 2016), the loess sequence is ~80 m thick. It thins toward the east and toward the west. The middle of the loess section is late Pleistocene in age (Machalett et al., 2006), but the last two peaks in loess deposition occurred around MIS 3 and during the LGM. These depositional periods left layers of ~8 m thickness (Fitzsimmons et al., 2016).

The loess-covered foothills of the range exhibit fault scarps with heights of 50–100 m (Figures 3 and 4). These scarps are abundant and can be found almost everywhere along the Zailisky Alatau. The thickness of the loess cover and the underlying bedrock morphology are mostly unknown, thus hampering any attempts to measure fault slip rates at the rangefront.

4. Active Tectonics Along the Rangefront

In this section we discuss the study sites S1–S11 in detail (Table 1). We work our way from west to east and report on morphological indicators of active faulting.

4.1. Western Zailisky Alatau

The Almaty rangefront fault intersects, in the west, the Dzhalaïr-Naiman Fault, a long NW–SE trending strike-slip structure that extends into the Kazakh platform (Figures 2 and 5). The range reaches an elevation of approximately 2,500 m here. An isolated plateau north of the rangefront, with elevations between 1,000 and 1,400 m, dips gently to the north between the latitudes 75.5° and 76°E. Incised streams (Figures 2 and 5) and a sharp drop in elevation indicate uplift along an ENE-oriented, S-dipping reverse fault (Figure 5). Basement rocks crop out in the hanging wall that sits about 150–400 m above the undeformed platform. The relief fades out toward the eastern end of the plateau, but gentle hills and incised streams can be identified as far as Almaty (Figure 2). These features indicate large-scale uplift that probably started relatively recently because the streams incise into the foreland sediments. The entire western part of the piedmont is covered by a layer of loess with varying thickness.

4.1.1. Akterek (S1 and S2)

Near the village of Akterek (russ. Акте́рек), the rangefront fault has uplifted the plateau surface described above. Basement rocks crop out in the hanging wall; a thin Cenozoic basin section is still preserved and crops out in the hanging wall. Topographic throw is up to 400 m. The rangefront fault turns to the NW at its western end. A number of small streams, some of them intermittent or ephemeral, drain the plateau to the north (Figure 5a). River Zhamanty (russ. Жаманты) is the largest perennial stream and has incised deeply into the uplifted plateau surface. It leaves the mountainfront at our study site S2. Different generations of alluvial fans can be distinguished based on their surface roughness, but none have been dated so far. Distinguishing by their elevation, modern day stream courses, and the degree of fan dissection, we grouped them into T1–T4 (youngest to oldest; Figure 5d). We expect the fan surfaces to be Late Quaternary in age, the youngest ones probably postdating the LGM (see also Thompson et al., 2002, and Burgette et al., 2017, and the references therein for Quaternary terrace sequences in the Tien Shan). Burial mounds (kurgans) are found on alluvial fans of all generations. These kurgans are probably not more recent than Iron Age (8th–4th Century BCE; Hall, 1997; Sala & Deom, 2005), which can thus be seen as a minimum age of the alluvial surfaces. A loess layer of varying thickness is present on top of all alluvial surfaces. All alluvial surfaces are truncated at the rangefront and thus interpreted to be vertically offset by the rangefront fault.

Table 1
Overview of the Study Sites Discussed in This Paper

Site	Coordinates	Type of deformation	Offset	Age	Slip rate	Comment	Figures
S1 Akterek	N43.211°, E75.573°	Offset alluvial fans	2.2–2.5 m	Unknown, probably ~LGM or Holocene, predates kurgans	—	Elevation profiles from drone DEM	Figures 5 and 6
S2 Akterek	N43.227°, E75.612°	Offset alluvial fans and river terraces	6–7 m	Unknown, probably pre-LGM, predates kurgans	—	Elevation profiles from drone DEM	Figures 5 and 6
S3 Fabrichny	N43.152°, E76.446°	Offset alluvial fan	1 m	Unknown, probably ~LGM or Holocene, predates kurgans	—	—	Figure 7
S4 Almaty	N43.239°, E76.948°	Offset alluvial fan	5–7 m	Unknown	—	Elevation profiles from SPOT6-DEM	Figure 9
S5 Talgar	N43.296°, E77.214°	Offset alluvial fan and folding (blind thrust)	5 m	Unknown	—	Elevation profiles from SRTM1 and JAXA DEMs	Figure 10
S6 Rahat	N43.368°, E77.371°	Offset river terraces	5–11 m	Unknown, youngest terraces probably Holocene	—	Elevation profiles from drone-DEM	Figures 11 and 12
S7 S5\$lip rate site near Chilik	N43.491°, E78.136°	Offset river terraces	9–50 m	Terrace with 14 m offset is 13.3–15 ka	1.2–2.2 mm/a in the Holocene	Elevation profiles from drone-DEM	Figures 14–17
S8 Big Almaty canal	N43.488°, E78.155°	Offset alluvial fans	Unknown	Unknown, probably ~LGM	—	—	Figure 18
S9 gravels east of Chilik	N43.498°, E78.270°	Deformed gravels–fault-propagation fold?	—	Unknown	—	—	Figure 19b
S10 alluvial fan east of Chilik	N43.505°, E78.490°	Offset alluvial fans	1–3 m, several higher scarps also visible	Unknown, probably ~LGM or Holocene, predates kurgans	—	—	Figure 19c
S11 Selander et al. (2012) study site	N43.432°, E78.298°	Offset alluvial fans	0.5–24 m	Youngest surfaces probably ~LGM or Holocene, older terraces estimated to be 100 ± 30 ka based on data from Q2 terraces in other parts of the Tien Shan (Selander et al., 2012)	0.8 ± 0.5 mm/a and 0.43 ± 0.3 mm/a (Selander et al., 2012)	Elevation profiles from DGPS data	Figures 21 and 22
Western Zailisky Alatau, peneplain south of Ushkonnyr	N43.089°, E76.499°	Fault scarps in peneplain surface	Unknown	Unknown	—	—	Figure 2
Uplift NW of Almaty	N43.310°, E76.811°	Uplift of the foreland sediments and stream incision, blind thrusts or folding	Unknown	Unknown	—	—	Figure 8
Kosmos	N43.531°, E77.281°	Folded and offset glaciofluvial deposits	Small-scale folding	17.1 ± 0.22 ka BCE	—	Site described and dated by Macklin et al. (2015)	Figure 8

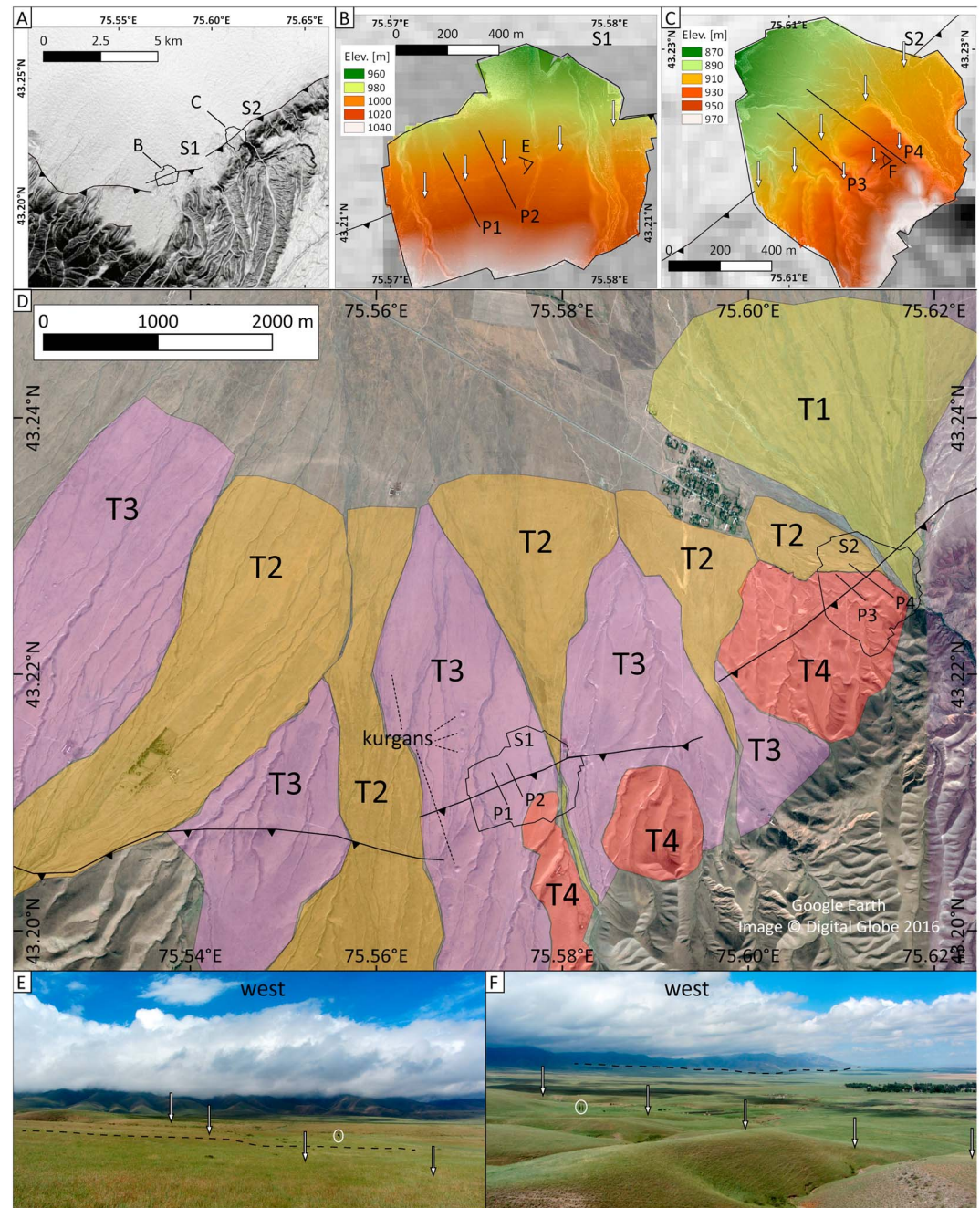


Figure 5. Akterek study sites S1 and S2. (a) Slope map based on SRTM1 data. Black lines are faults, A and C indicate the location of the two drone DEMs of S1 and S2 in Figures 5b and 5c. (b) Drone DEM with 0.1 m resolution at S1, overlain with a semitransparent slope map. Arrows mark the fault scarp. P1 and P2 mark the two profiles in Figures 6a and 6b. E marks view direction of photo in Figure 5e. (c) Drone DEM with 0.1 m resolution at S2, overlain with a semi-transparent slope map. Arrows mark the fault scarp. P3 and P4 mark the two profiles in Figures 6c and 6d. F marks view direction of photo in Figure 5f. The NE–SW striking linear feature visible at the NW end of P3 is a goat track. For this reason we do not label it in Figure 6. (d) Alluvial fan surfaces T1–T4 at sites S1 and S2. T1 is the modern riverbed, and T4 is the oldest fan. (e) Photo of the fault scarp at S1 looking west. White arrows mark the fault trace, dashed line is profile P2, person for scale (encircled). (f) Photo of the fault scarp at S2 looking west. White arrows in the foreground mark the fault trace at the study area, dashed line traces the NW striking fault trace in the background. Five meter high poplars are encircled for scale.

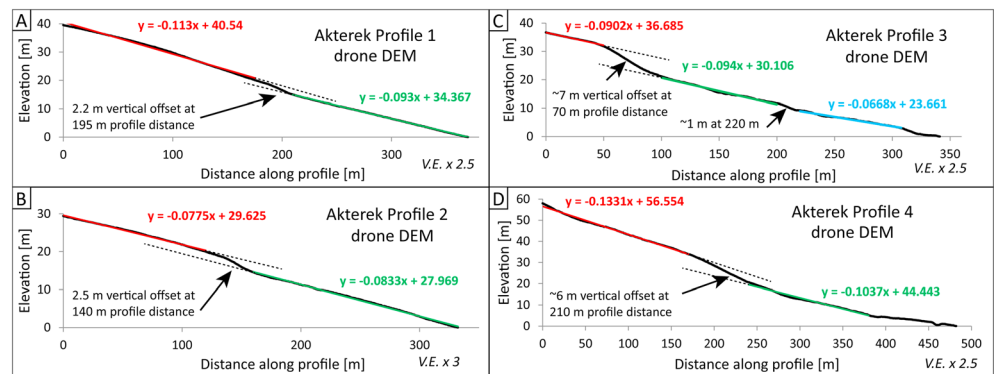


Figure 6. Topographic profiles at sites S1 and S2 near Akterek. (a) At S1 the fault scarp shows a vertical throw of 2.2 m in surface T3. (b) Fan T3 has a vertical offset of 2.5 m as observed in profile P2. (c) At S2 we observe ~7 m vertical throw at a profile distance of 70 m and another 1 m throw at 220 m profile distance in profile P3. This profile covers fan surface T4. (d) A vertical throw of ~6 m is observed in profile P4. Here the hanging wall is fan surface T4, and the footwall is T3. Note that we plot elevation differences instead of absolute elevations.

We observed N-facing fault scarps (Figure 5) that offset at least three generations of alluvial fan surfaces T2–T4 except the modern riverbeds T1. The western section is oriented W(NW)–E(SE) and joins the NW-trending fault. The scarps in the east are subparallel to the strike of the range-front fault and strike NE. All scarps are degraded, and no fresh surface breaks were observed. We analyzed two high-resolution drone DEMs that capture the scarp at S1 and S2, respectively.

At study site S1, the offset can be traced for ~2 km in the T3 and T4 surfaces. We observe a relatively uniform throw of 2.2–2.5 m (Figures 6a and 6b). Note that we only show two representative profiles here. The scarp is located ~1.5 km north of the main topographic step. Judging by the degradation of the scarp and comparison with studies from other sites in the region (Grützner et al., 2017; Landgraf et al., 2016; Thompson et al., 2002), we suspect that one or more Holocene earthquakes caused the offset.

Study site S2 is located further NE along the same scarp system at the mouth of River Zhamanty. Fan surfaces T3 and T4 contain abundant kurgans. T4 is dissected by ephemeral streams that have incised into the alluvium. We have no direct age control of T4, but its morphology suggests that it is much older than T2 and T3, though probably Late Pleistocene based on similar morphology of dated surfaces elsewhere in the Northern Tien Shan (Burgette et al., 2017; Thompson, 2001; Thompson et al., 2002). The fault scarp is degraded at site S2 relative to S1 but continuous for ~1.5 km. It forms the NE continuation of the scarp at site S1 and lies ~500 m away from the main topographic step. Vertical throw on T4 is ~7 m with a smaller scarp of ~1 m height present further downslope (Figure 6c). A second nearby profile across the T4 fan surface identifies a throw of 6 m. This offset was found at the contact of two different fan generations (Figure 5d). The scarp heights at S2 are similar within their error bounds but consistently higher than at S1. This variation in height may indicate that the topographic step was formed by multiple earthquakes. Based on the morphology and the scarp heights at sites S1 and S2, we suggest that the offset of T3 represents the most recent surface rupturing earthquake(s), which probably did not occur in the past few hundred years, but likely after the LGM. T4 has recorded multiple events based on its scarps being several times the height of T2 and T3 scarps.

4.1.2. Fabrichny (S3)

Site S3 lies at the piedmont south of the town of Kargaly (russ. Каргалы), the former Fabrichny (russ. Фабричный). A small perennial stream exits the mountains here and incises deeply into the loess that covers the mountain front. These hills show a sharp break in slope (black arrows in Figure 7a). The morphology of the landform suggests that this is a fan, with sediment composed of loess reworked from higher elevations in the catchment. The stream has a small catchment that only encompasses the degraded mountain slope below the peneplain surface (~900 m above the Kazakh platform; Figure 2a). As the stream incises into the loess cover, mass wasting processes dominate the sediment supply in large parts of the catchment. The loess has an unknown thickness, as outcrops observed in nearby riverbanks do not expose any other material.

At least four kurgans can be identified on the alluvial surface in declassified Corona satellite imagery from 1969 (Figure 7a). Those burial mounds are not likely to be younger than Iron Age (Sala & Deom, 2005).

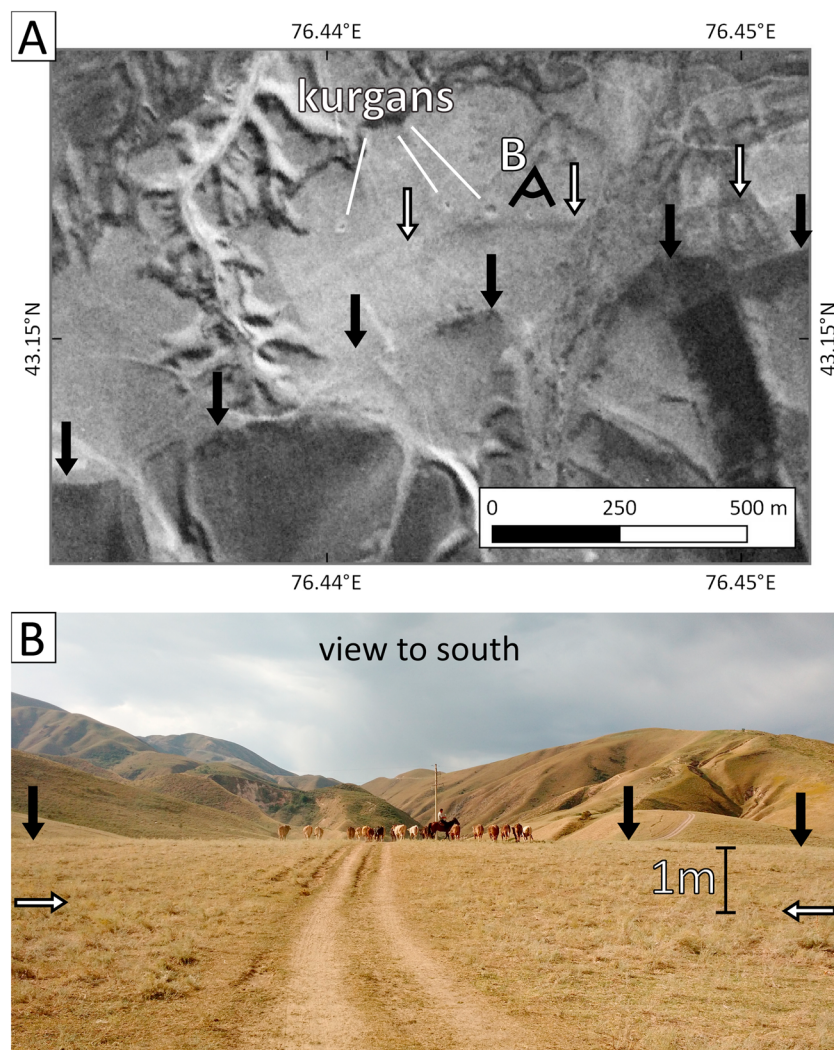


Figure 7. The Fabrichny study site (S3). (a) Declassified Corona imagery from 1969 has the advantage of predating the latest phase of urban development that began in 2012/13. Black arrows indicate the ~50 m high scarp in the loess-covered foothills. White arrows mark the 1 m high fault scarp. Note the kurgans N of the scarp. B marks the location of the photo shown in Figure 7b. (b) The fault scarp (white arrows) faces to the north and is degraded.

Currently, the archeological remains are less visible because the site is being developed for private housing. We found a N-facing, ~1 m high fault scarp that offsets the youngest alluvium (white arrows in Figure 7b). The scarp runs ENE for at least 700 m, is marked by a gentle break in slope, and has a rather uniform height. Due to the housing project, the scarp is more visible in 1960s Corona satellite images than in modern imagery (Figure 7a). We interpret the scarp as the surface expression of the most recent surface-rupturing earthquake(s). The scarp morphology suggests that the offset was produced after the LGM, probably several hundreds or thousands of years ago. Fabrichny is located in the epicentral area of the 1887 Verny earthquake ($M7.3$) that is not known to have ruptured the surface. However, it remains unclear whether the 1887 earthquake ruptured the fault we investigated but did not reach the surface, or if it occurred on some unknown fault in the mountains.

4.2. Central Zailisky Alatau

The central part of the Zailisky Alatau is characterized by higher elevations of 3,000–4,000 m west of Almaty. Further east, even higher elevations are present, and the almost 5,000 m high peak Talgar 30 km SE of Almaty is the highest in the range (Figure 4). The peneplain surface is well preserved in this part of the Alatau (Figure 2). It has a width of approximately 5 km and is tilted toward the north. The peneplain occupies an

altitude range of 2,000–2,500 m in the western part and lowers to a range of 1,200–1,800 m in the eastern parts near Almaty, where it disappears. Further east, a few patches of peneplain-like plateaus can be found between the high Zailisky Alatau and the Kazakh platform, but in general, they are more heavily eroded, have a higher internal relief, and are less continuous than in the west.

Within the peneplain, ENE-striking scarps near Ushkonyr are obvious in satellite imagery and in the DEM (Figures 2c and 3). These scarps face SSE, have a height of several meters, and are up to 10 km long. North of the scarps, incision of the streams testifies to uplift, while south of the scarp only relatively minor incision is evident. This is consistent with decreased stream power due to the aggradation of sediment against the scarp. These lineaments are interpreted as backthrust faults since they are parallel to the mountain front and to the main strike of the ridge, which suggests that they are structurally related to the uplift.

4.2.1. Almaty (S4)

Almaty is mainly built on the alluvial fans of four rivers that drain the Zailisky Alatau and increasingly occupies the loess-covered foothills in the south (Figures 4 and 9). This urban development makes it difficult to identify any geomorphological indicators for active faulting. The main roads in Almaty run in a system orthogonal to the drainage directions. Since the roads are relatively wide, they are good targets to measure topographic profiles along them. Along one of the N–S running main roads, Ul. Furmanova, we observed in the field a break in slope just north of the intersection with the E–W running Ul. Satpayeva (43.239927°N; 76.948643°E). This feature is also visible in digital topography (Profile P2 in Figures 9a and 9b).

In order to test whether or not this is a north-facing scarp of tectonic origin, we analyzed the freely available SRTM1 (NASA) and ALOS (JAXA) topographic data sets. In the JAXA DEM hillshade map, it is clear that the break in slope is a linear feature that can be traced across the alluvial fan (Figure 9a). To measure the offset across the scarp, we extracted the elevation data along three N–S running main roads: Ul. Seyfullina (P1), Ul. Furmanova (P2), and Ul. Dostyk (P3; from west to east in Figure 9).

The scarp in P1 cannot be identified in the SRTM1 data (Figure 9c) but is just visible in the JAXA DEM (Figure 9d). Neither SRTM1 nor the JAXA DEM can reveal the scarp in P2 (Figures 9g and 9h) and P3 (supporting information Figure S1). The relatively poor resolution of the data sets ($\sim 30 \times 30$ m) is not suitable to resolve such tectonic features in an urban environment, even if it can be recognized on a hillshade map.

To overcome the issue of the low resolution, we acquired SPOT6 stereo satellite imagery and extracted the elevation data of the same three profiles P1–P3. Although we centered the profiles on the middle of the wide Almaty streets, the data show spikes (Figures 9e and 9i; supporting information Figure S1). This is most likely caused by the nearby multistorey buildings and trees. However, straight lines fitted to the profiles on either side of the scarp location, as identified in the field and in the JAXA DEM, reveal a significant vertical offset. In profile 1, the vertical offset is ~ 5 m (Figure 9f), whereas it is ~ 7 m in profile 2 (Figure 9j). No offset was detected in profile 3 (supporting information Figure S1). We interpret the feature as the surface expression of active reverse faulting for two reasons: (i) The scarp clearly offsets the entire alluvial fan and is visible in two profiles more than 1 km apart. This rules out local building ground modifications or other anthropogenic cause. (ii) The scarp aligns with the main mountain front on either side. A more detailed morphological investigation of the scarp in the field is impossible since it is located in the heart of the city.

On a wider scale, the drainage pattern indicates a broad region of uplift of the foreland sediments west of Almaty. We find an arched/warped surface into which streams and rivers incise (Figure 8). The uplift manifests in the field only as gently sloping hills, but it is clearly discernible in the slope map. In addition to this general pattern in the west and northwest of Almaty, there are narrower anticlinal structures with NE trends in the northern outskirts of the city (Figure 8). We observe pronounced incision into the foreland sediments here. The riverbanks are almost vertical walls of several meters height. Individual anticlines can be distinguished, and the general morphology indicates rather recent uplift. This structure implied deformation above a thrust fault that must underlie the city. In the platform northeast of Almaty, there are no topographical signatures of active tectonics. However, Macklin et al. (2015) report deformed fine-grained glaciofluvial deposits of post-LGM age (Figure 8b) near Kosmos. Radiocarbon dating of an organic-rich layer yielded an age of 17.1 ± 0.22 ka cal BCE. These layers are folded on a 1 m scale. They are not likely to represent liquefaction structures because the deformation is only found here and is not widespread in these layers. Similarly, we rule out glacial deformation features or a slump: the slope is very shallow—the layers are almost horizontal—and the deformation is localized. We interpret the deformed layers as indicative of compression caused

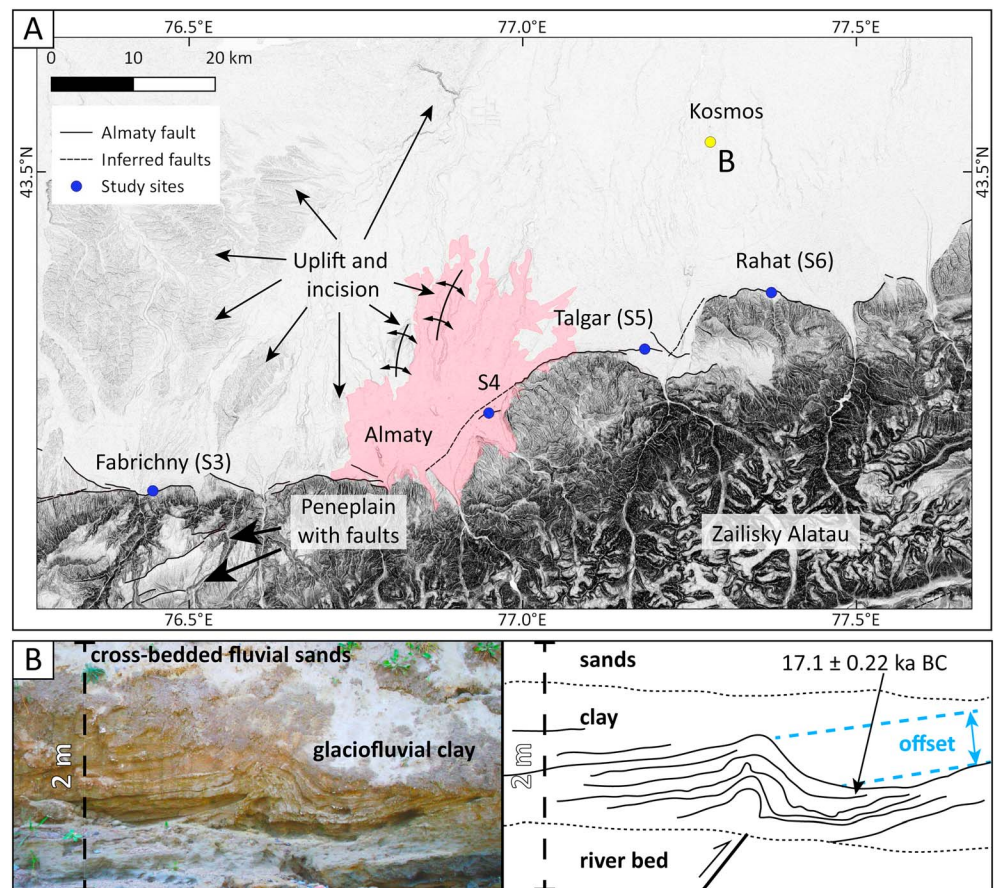


Figure 8. (a) Slope map of Almaty from SRTM1 data. The drainage pattern to the northwest of the city indicates active uplift and consequent incision of the streams. Faulting is not confined to the range front but also observed in the penneplain. Pink shading denotes the outline extent of the urban development. (b) At the Kosmos reach of river Talgar, Macklin et al. (2015) found folded and offset (blue lines) glaciofluvial deposits with an age of ~ 17 ka, overlain by undeformed units. Photo by Willem Toonen.

by a small-scale fault-propagation fold on top of a thrust fault that takes up shortening in the foreland. The fact that no deformation is detectable in the 30 m DEM would confirm the observation made elsewhere that the recurrence intervals of large surface-rupturing earthquakes are typically long and that surface deformation features are rapidly obliterated by sedimentary processes. In this case, the deformed layers were found in a reach of the Talgar River that drains a large catchment of the Zailisky Alatau and has a high sediment load.

4.2.2. Talgar (S5)

The Talgar River drains the highest peaks of the Zailisky Alatau and is fed by a number of glaciers. A dam is located 1 km upstream of the mountain front to mitigate floods and mudslides. To the west and east of the river, small remnants of the penneplain are possibly preserved, although they are intensely incised. The city of Talgar (russ. Талгар) is built on the alluvial fan of the Talgar River and has, similar to Almaty, seen a recent spike in urban development. Due to the presence of the city, it is not clear if there are different generations of alluvial surfaces here. The foothills behind the city form 100–300 m high, relatively steep fronts and are covered in loess of unknown thickness. Exposures within recent landslides observed in the field constrain that the loess exceeds 20 m thickness. Between Almaty and Talgar, housing projects have started to develop those loess-covered foothills. East of the mouth of the river, a relatively smooth surface surrounded by higher mountains is tilted toward the west (Figures 8 and 10).

We did not observe any fault scarps cutting the Talgar alluvial fan during our field survey. In order to check if there is large-scale evidence of active tectonic deformation preserved in the landscape, we analyzed the SRTM1 and JAXA ALOS DEMs (Figure 10) after our fieldwork. We calculated elevation, slope, and TRI maps

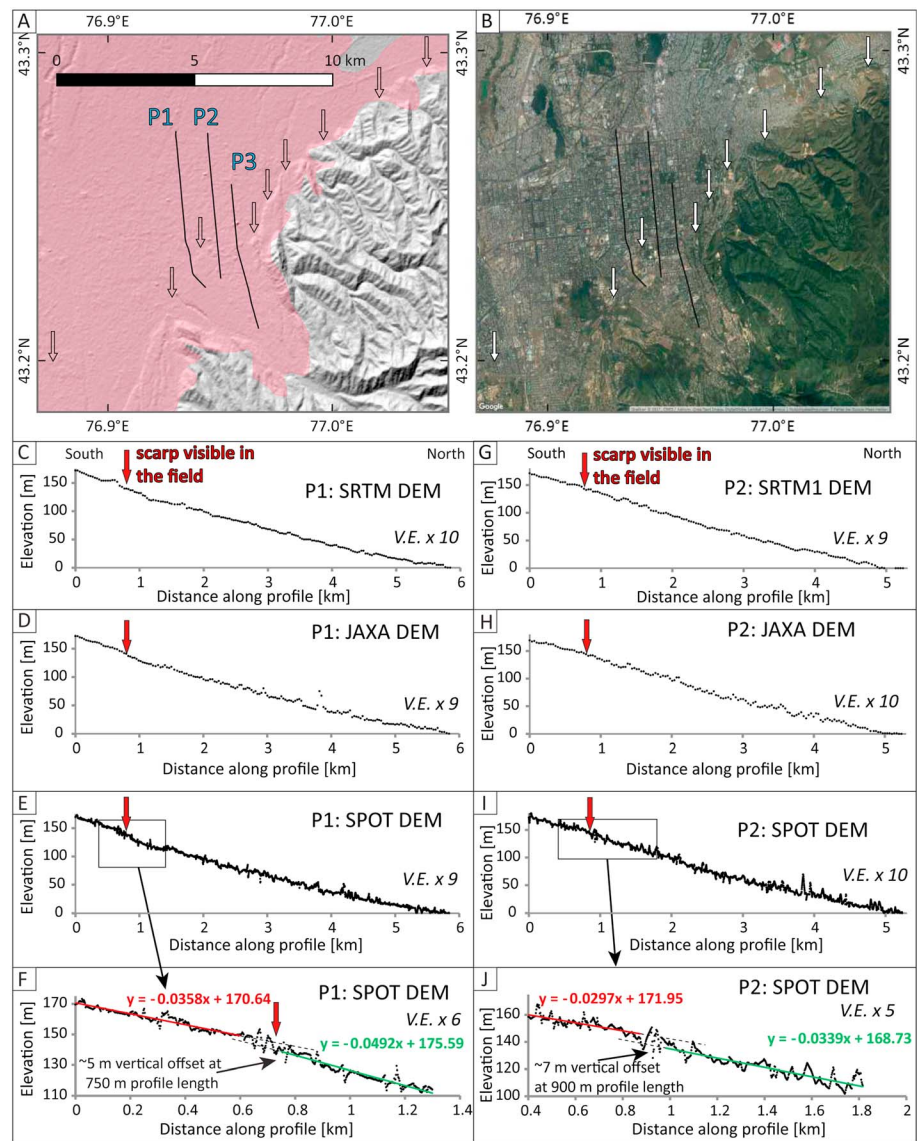
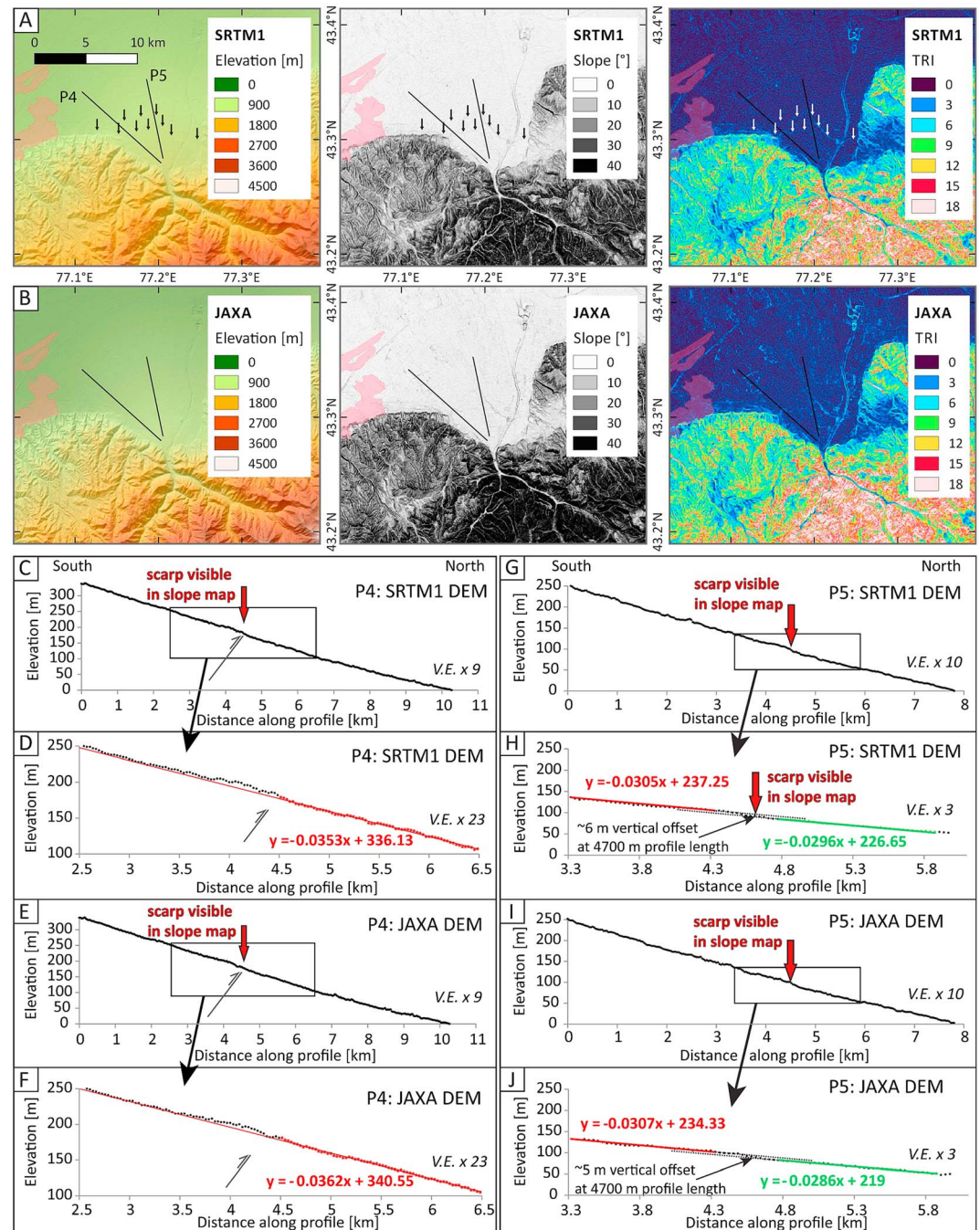


Figure 9. Fault scarps in Almaty (site S4). (a) The JAXA DEM hillshade map reveals a linear break in slope across the alluvial fan (arrows). P1–P3 mark the location of the topographic profiles along main roads. Pink shading denotes the outline extent of the urban development. (b) Same map as in Figure 9a but with Google Earth satellite imagery. (c) Topographic profile P1 from SRTM1 data. (d) Topographic profile P1 from JAXA data. (e) Topographic profile P1 from the SPOT DEM. (f) Zoom into the SPOT DEM along P1. (g) Topographic profile P2 from SRTM1 data. (h) Topographic profile P2 from JAXA data. (i) Topographic profile P2 from the SPOT DEM. (j) Zoom into the SPOT DEM along P2. In all profiles the red arrow marks the location of the scarp as seen in the field.

of both data sets and identified lineaments that cross the alluvial fan at high angle to the drainage direction. These lineaments align with the mountain front in the west and the northern edge of the smooth plain in the east (arrows in Figure 10a; for a clearer view, the arrows were left out in Figure 10b).

Elevation data were extracted along two profiles P4 and P5 and processed as described in section 2. The profiles run parallel to the drainage direction in order to avoid crossing different fan generations. Profile P4 does not reveal a sharp break in slope at the location of the scarp. Instead, we observe a broad zone of folding with a wavelength of ~1 km (Figures 10c–10f). This structure can be identified in both the SRTM1 and the JAXA DEMs. The surface of this anticline deviates up to ~5 m from a straight line fitted to the upslope and downslope sections on either side of the fold. The section uphill of the fold in profile P4 is also systematically offset with respect to the section downstream of the fold.



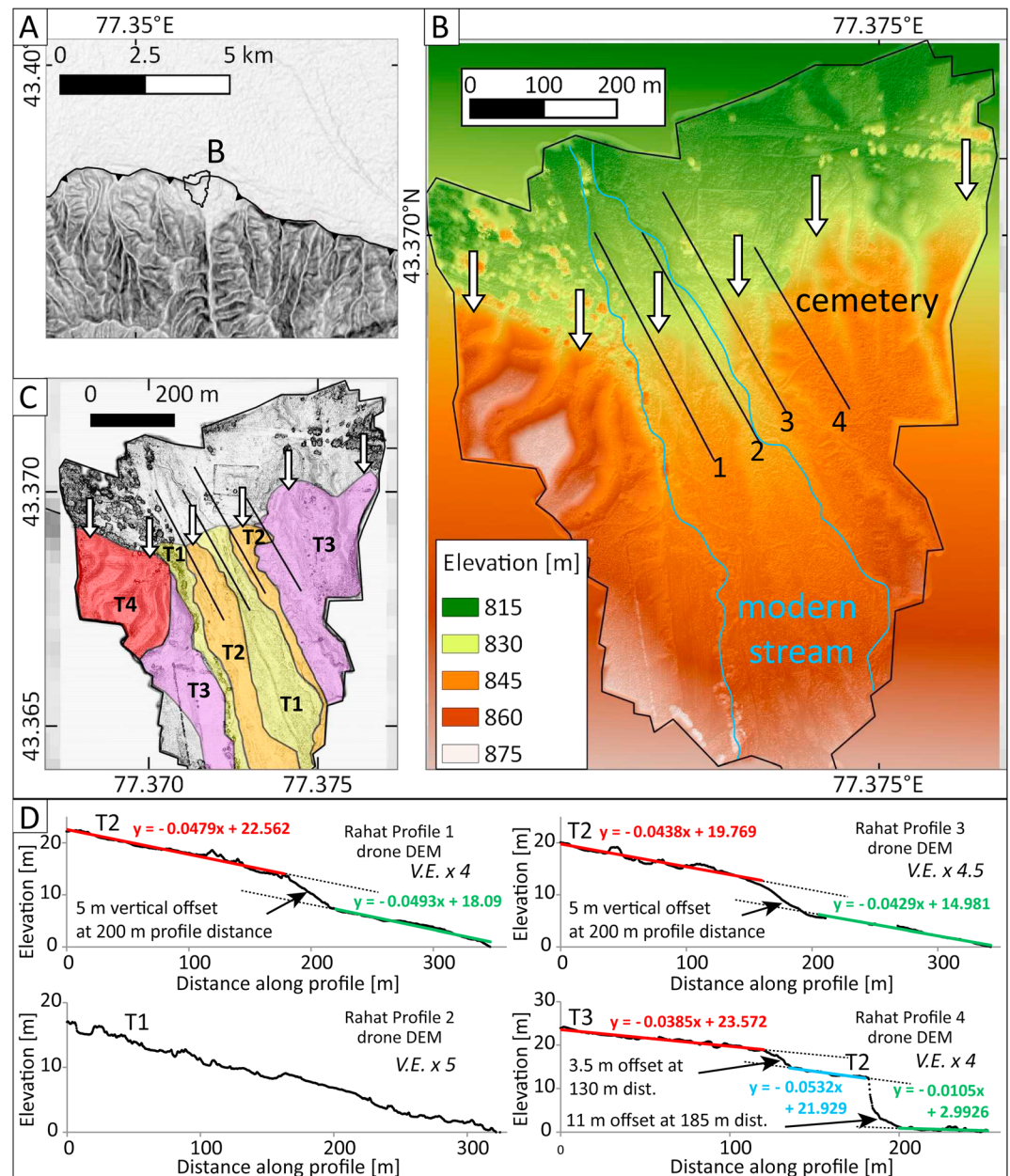


Figure 11. Study site S6 near Rahat. (a) Location of the study site (black outline) on a SRTM1 slope map. (b) Drone DEM of the study site overlain with a semitransparent slope map with the four profiles shown in Figure 11d. White arrows mark the fault scarp. (c) Slope map from the drone DEM with the three river terraces T1–T4 (youngest–oldest). (d) Topographic profiles 1–4 extracted from the drone DEM.

Profile P5 exhibits a change in slope angle where we identified the lineament in the slope map (Figures 10g–10j). We observe ~6 m vertical offset in the SRTM1 data (Figures 10g and 10h) and ~5 m vertical offset in the JAXA DEM. It is not clear whether this feature is a highly degraded fault scarp, that is, an ancient surface rupture, or related to a monocline/anticline structure above a blind fault. The presence of the anticlinal structure in P4 makes it likely that P5 also records blind faulting. Such features can hardly be seen with the naked eye or in imagery but are clearly expressed in topographic data.

The observed folding in the Talgar fan is interpreted as the surface expression of a blind thrust fault that caused a fault-propagation fold in the overlying sediments. We cannot assign an age to the structures but suspect them to be several thousand years old. The lack of any more distinct tectonic landforms may be

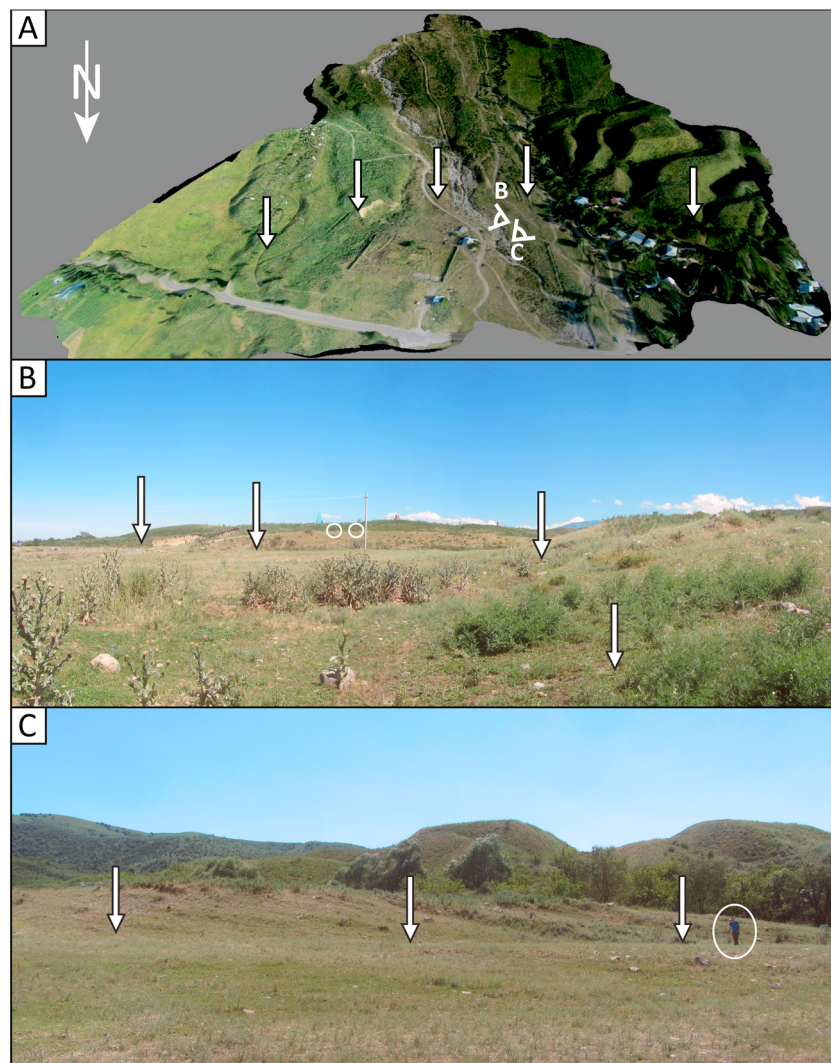


Figure 12. Field photos of the scarp (white arrows) in Rahat. (a) Aerial imagery draped over the drone DEM. Capital letters indicate location and direction of photos in Figures 11b and 11c. (b) View east toward the cemetery. Horses encircled for scale. (c) View to the southwest toward profile 1 in Figure 11. Person encircled for scale.

explained by the prevalence of loess that accumulates against the piedmont and/or by a period of relative tectonic quiescence. We cannot distinguish between these two alternatives without further investigation.

4.2.3. Rahat (S6)

Rahat (russ. Paxar) is a settlement that is situated at the mouth of a perennial stream that occupies a rather wide and linear valley. An alluvial fan formed at the base of the mountain front, the western half of which is occupied by the village. The foothills south of Rahat are covered in loess and reach up to 500 m above the elevation of the Kazakh platform, with a ~50 m high scarp in the loess-covered hills marking the northernmost edge of the mountain front (Figure 11).

At our study site the mountain front is embayed to the south and occupied by a flat-bottom valley of a north-draining catchment from the Zailisky Alatau (Figure 11b). At the western edge of the valley, we find a loess-covered surface that forms the oldest of a series of river terraces (T4). The T4 terrace surface has been modified, with the construction of an earth mound surrounded by two square ditches. The age of this archaeological site, and the terrace on which it sits, is unknown as far as we know. The east flank of the valley is occupied by a cemetery situated on a lower terrace level T3 (Figure 11c). The same terrace is also preserved as a narrow strip along the western riverbank. Apart from the present-day riverbed T1, we identified another river terrace T2 (Figure 11c) in the center of the valley.

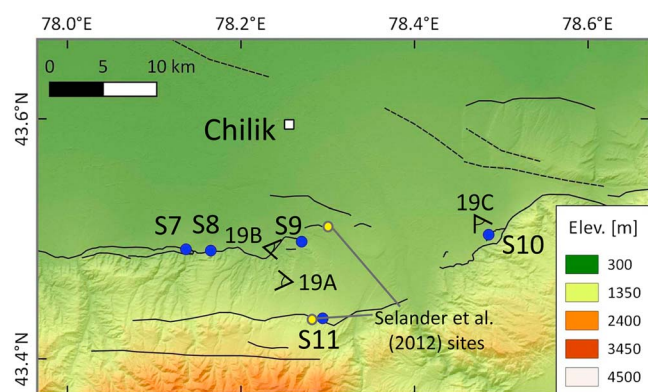


Figure 13. Investigation sites at the eastern end of the Zailisky Alatau range front near Chilik. Overview map showing the study sites S7–S11 (blue dots). Yellow dots indicate the slip rate site of Selander et al. (2012). Black lines are active reverse faults mapped remotely or in the field. Dashed lines are active faults inferred from gaps in between the mapped fault traces. Capital letters and symbols mark the location of photos in Figure 19.

A fault scarp in different stages of degradation is visible in the field (Figures 11 and 12). The entire lower part of the valley was and still is subject to anthropogenic interference. Channels and weirs have been built for irrigation and various dirt roads wind around excavated material. These features make it difficult to properly assess the scarp height. We therefore produced a DEM from drone imagery with the methods described in section 2. The DEM has a resolution of ~ 0.1 m. Despite the complicated surface conditions, the scarp is visible as a continuous feature across the valley, except in the modern streambeds.

We extracted the elevation along four profiles from different terrace surfaces in the valley (Figures 11b and 11c). Profiles 1 and 3 show ~ 5 m offset across the scarp. These profiles are situated on the lowest (= youngest) surface that is affected by the offset, T2. Profile 2 is from the modern riverbed T1 and exhibits neither a scarp nor a retreated knickpoint in this surface (Figure 11c). The highest (= oldest) terrace level that we investigated, T3, is offset at two locations (profile 4). At 130 m profile distance, we observe 3.5 m of vertical offset. Another 11 m of vertical offset was found at the northern end of the profile at

a loess quarry. The shape of the scarp is anthropogenically modified, but the total vertical throw of 11 m is measured between adjacent intact fluvial surfaces.

We interpret the scarp to be caused by thrust faulting in past earthquakes. It is impossible to distinguish between single-event and multi-event scarps due to the poor state of preservation (Figures 11 and 12). Past reverse faulting earthquakes in the Tien Shan have produced offsets of more than 5 m (e.g., Abdrakhmatov et al., 2016), but it is not clear whether the lower scarp can be assigned to a single event. The difference in the vertical offsets of different fluvial terraces (i.e., between the two profiles 1 and 3 and profile 4) indicates that more than one earthquake is recorded in the landscape. The older (= higher) terrace surface T3 was probably uplifted by at least one additional event compared to the lower terrace T2. Neither of these surfaces has been dated, but the state of preservation indicates that the surface ruptures probably happened after the LGM, likely in the Holocene.

4.3. Eastern Zailisky Alatau

East of 77.5°E , the Zailisky Alatau reaches elevations of less than 3,000 m. The range front is sinuous here and curves around the rather wide valleys carved by the main rivers. Straight mountain fronts are often interpreted as tectonically active, while sinuous ones tend to indicate lower grades of tectonic activity or inactivity (Bull & McFadden, 1977). A possible alternative explanation for this observation is the higher discharge of the main rivers compared to those in the central and western sections of the range front. It is unclear if the higher sinuosity of the range front is entirely due to a higher erosional power of the streams or rather caused by lower uplift rates. The basement geology is not significantly different from other parts of the range front, which makes it unlikely that lithological changes (less/more resistant to erosion) can explain the observations. In the foreland north of the eastern section, there are no morphological hints that would clearly indicate uplift. Several parallel fault strands can be identified in the easternmost parts of the mountain front (Figure 13). Here Selander et al. (2012) report offset and deformed Q2 terraces giving tentative slip rates of 0.8 ± 0.5 mm/a and 0.43 ± 0.3 mm/a for the two parallel faults, respectively (Figures 1b and 13). While the offsets were measured in the field, no direct dating of the surfaces was performed. An age of 100 ± 30 ka was assumed based on data from Q2 terraces in other parts of the Tien Shan dated by Thompson et al. (2002) and Bowman et al. (2004). This slip rate, therefore, has to be taken as an estimate because the ages were not verified by direct Quaternary dating, although the assumptions are reasonable. In the east, the Zailisky Alatau diminishes in the Ili Basin.

4.3.1. Slip Rate Site near Chilik (S7)

4.3.1.1. River Terraces

Site S7 is located near Chilik (Russ. Шенек) at the mouth of a stream that crosses a plateau of 1,100–1,200 m elevation between the Zailisky Alatau and the Kazakh platform. Here the Big Almaty Canal runs in front of the loess-covered foothills (Figure 13). We found a series of four river terraces preserved here (Figures 14 and 15).

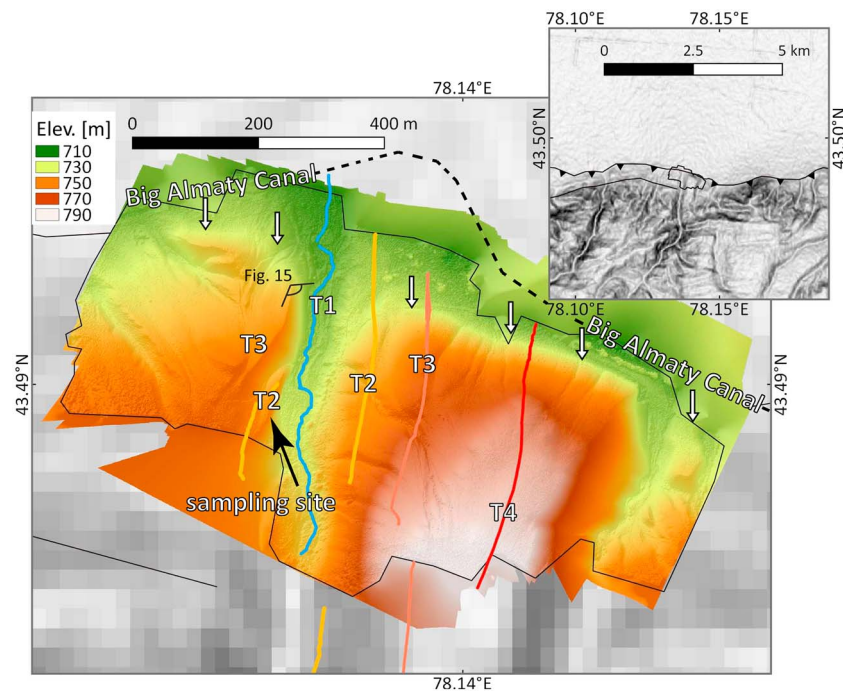


Figure 14. Study site S7. Inset shows the location of the site at the range front. The large map shows the drone DEM overlain with a semitransparent hillshade. Colored lines are the DGPS profiles on three different terrace levels; see Figure 16 for results. The blue line is the modern stream incising into T1. The big Almaty Canal is indicated by the dashed black line. White arrows mark the fault trace. See Figure 17 for a detailed view of the sampling site.

The oldest and uppermost terrace T4 forms the flat top of a $\sim 200 \times 400$ m wide hill at the right bank of the river. Terrace T3 is preserved as a flat, elongated surface at the right bank of the stream and as an incised remnant at the left bank. Terrace T2 is best preserved east of the stream, but an ~ 100 m long and 15 m wide section is also seen on the west side. T1 is the modern streambed. We interpreted those terraces as geomorphological markers that would allow us to determine the vertical uplift rate of the range front fault. This site is the best target for measuring a long-term slip rate that we were able to find along the entire mountain front.

In order to determine the vertical offset across the fault and to correlate the terraces, we acquired a photogrammetric DEM with the method described above (Figure 14). We also measured profiles on top of the terrace surfaces with DGPS (colored lines in Figure 14). Due to the nearby canal, the footwall profiles are much shorter than those on the hanging wall. The steepest part of the fault scarp was set as the fault location, and the vertical throw was measured here. Since the terrace surfaces are almost exactly parallel to the present-day riverbed, another choice (e.g., the base of the scarp or the center) would not result in a significant change in measured throw. We find a vertical offset of 50 ± 1.3 m in terrace T4 and 30.4 ± 1.6 m in terrace T3 on the east side of the stream (Figures 15 and 16).

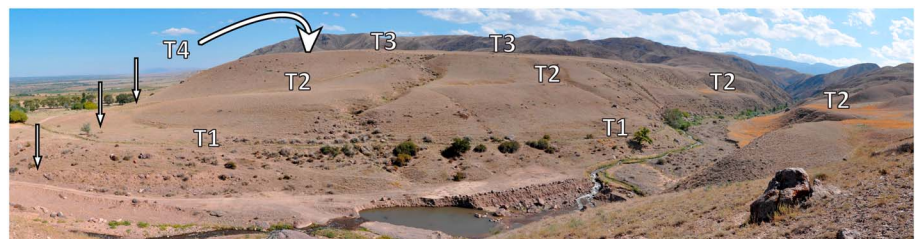


Figure 15. Panorama photo of the terrace levels at site S7 looking east. T4 is hidden behind T3 and not visible in this picture. The sampling site is not visible here as it is located below T2 in the foreground on the west bank of the stream. White arrows denote fault trace.

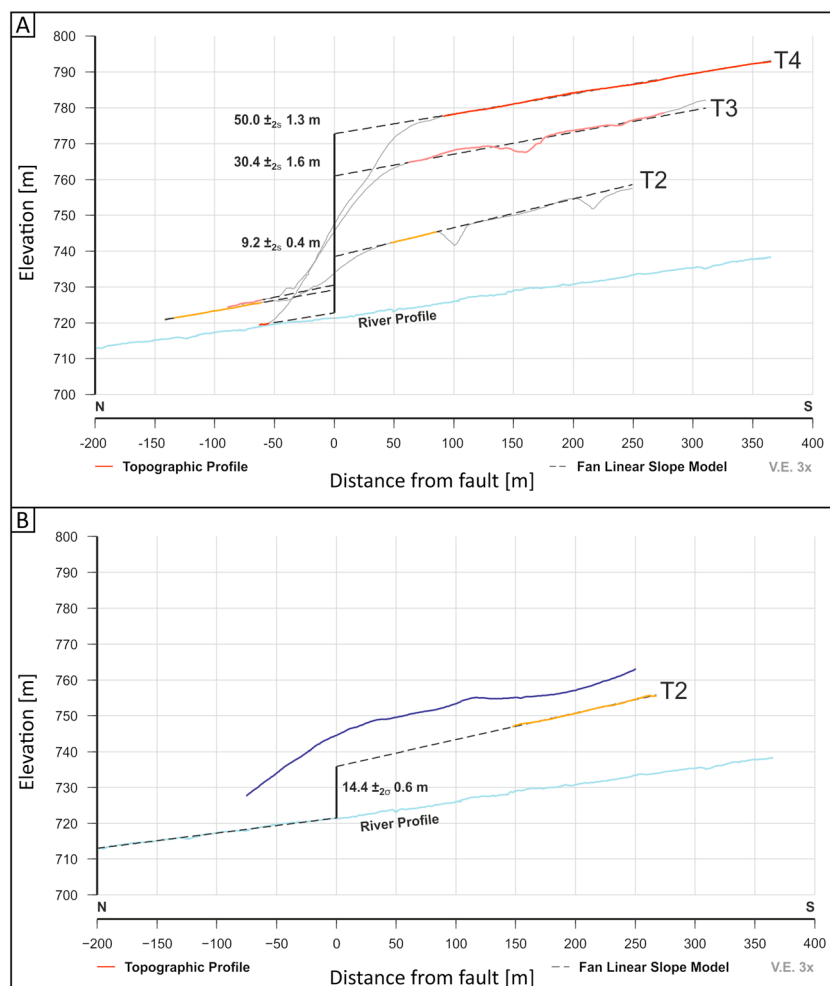


Figure 16. DGPS profiles across the different terraces with 3X vertical exaggeration; see Figure 14 for location. (a) Terraces on the eastern bank of the stream color coded as in Figure 14. We assumed a linear slope that we projected to the fault and then measured the vertical offset with respect to the footwall terrace or modern stream level. Fault location was set to the steepest section of the scarp. (b) Terrace profile T2 at the study site on the west bank of the stream. The purple line marks a remnant of a surface west of terrace T2.

Terrace T2 is offset 9.4 ± 0.4 m on the east side of the stream (Figure 16a), where it can be traced both in the hanging wall and in the footwall. The terrace is offset by 14.4 ± 0.6 m on the west side of the stream compared to the present-day streambed (Figure 16b). All errors are reported as 2σ as calculated from the linear fit.

We conclude that the terraces have been consequently uplifted by the mountain front thrust fault in multiple earthquakes. It is not possible to directly correlate the uplifted surfaces in the hanging wall with their counterparts in the footwall, because any information on sedimentation in the footwall is lacking. However, the absence of incision in the footwall and the rather smooth surface indicate that deposition prevails here instead of erosion. Thus, the amount of uplift must be taken as minimum value, although there was probably rather little fluvial deposition adjacent to the present-day mouth of the river. The thickness of the loess is unknown here.

4.3.1.2. Radiocarbon Dating

We dated terrace T2 to calculate the uplift rate (Table 2). The stratigraphy of terrace T2 is exposed in a 10 m high vertical wall carved by the stream (Figure 17). The lowest part of the outcrop exhibits a 2 m thick layer of reddish medium to coarse gravels that dip 35° to the north (Figure 17b). This dip angle is much steeper than that observed at the terrace surface and indicates that the gravels were tectonically tilted before terrace

Table 2
Results From ^{14}C Dating of the Three Samples at Site S7^a

Sample	Lab code	Material and pretreatment	$\delta^{13}\text{C}$	Conventional age	2 σ calibration	D^{14}C
chilik-2016-upper	Beta443448	Organic sediment: acid washes	−21.7	12,770 ± 70 B.P.	Cal BCE 13,410 to 13,125 (cal B.P. 15,360 to 15,075)	−796.0 ± 1.8‰
chilik-2016-middle	Beta443449	Charred material: acid/alkali/acid	−23.7	11,470 ± 50 B.P.	Cal BCE 11,475 to 11,265 (cal B.P. 13,425 to 13,215)	−760.2 ± 1.5‰
chilik-2016-lower	Beta443450	Charred material: acid/alkali/acid	−25.5	11,580 ± 150 B.P.	Cal BCE 11,785 to 11,165 (cal B.P. 13,735 to 13,115)	−763.4 ± 4.4‰

^aDating was performed by BETA analytic (Miami, FL, USA). INTCAL13 was used for calibration (Reimer et al., 2013).

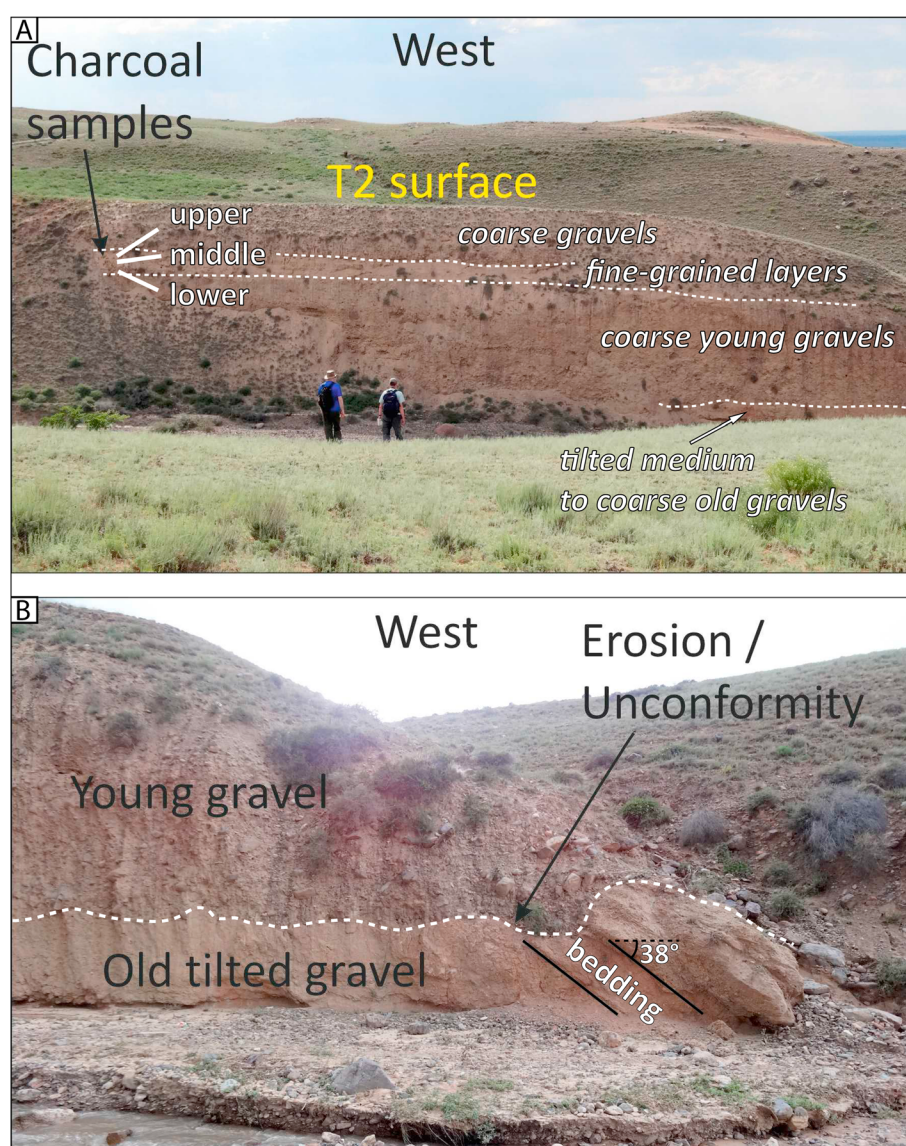


Figure 17. Sample location for the slip rate measurements. (a) Terrace T2 is covered by a 1 m thick gravel layer that overlies a fine-grained sequence. Three charcoal samples were taken from various depths below this gravel layer: chilik-2016-upper (0.8 m below); chilik-2016-middle (0.95 m below), and chilik-2016-lower (1.7 m below). See Table 2 for results. View is to the west. (b) The northern tip of T2 exhibits an erosional unconformity, separating Holocene gravels on top from N-tilted finer gravels of unknown age.

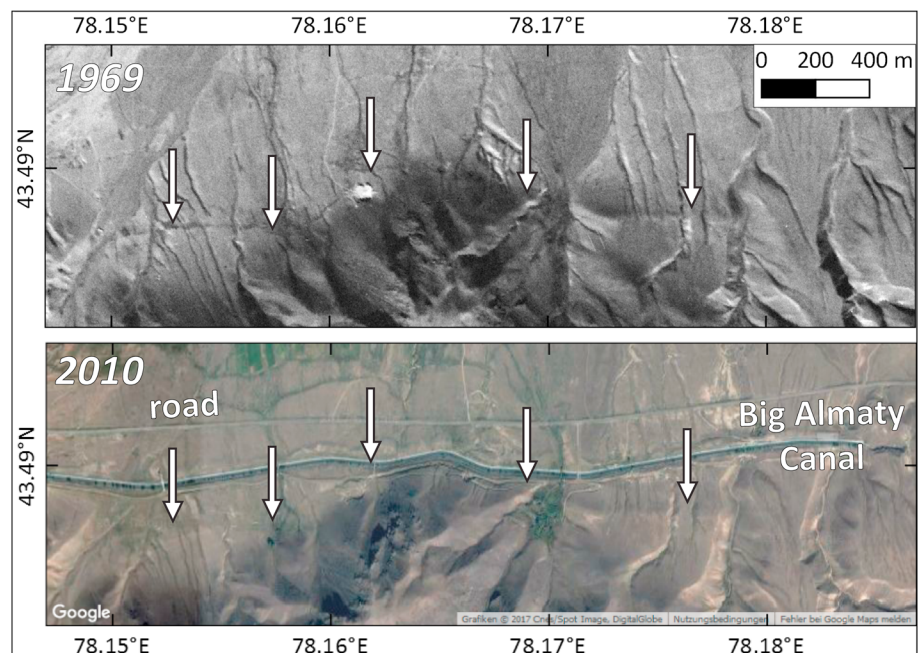


Figure 18. Site S8 at the Big Almaty Canal. A fault scarp is visible in declassified Corona satellite imagery from 1969. GoogleEarth imagery from 2010 shows that the canal was built along, and in parts on, the fault scarp.

formation. An erosional unconformity marks the top of this unit. The gravels are overlain by an 8 m thick sequence of subhorizontal, layered coarse gravels with boulders in a silty matrix. These high-energy deposits indicate episodes of alluvial aggradation. A fine-grained unit of ~2 m thickness follows on top. These fine-grained sediments consist of several layers of silty material and fine-medium sands, corresponding to a phase of low-energy transport. Three of those fine-grained layers contain numerous fragments of charcoal of up to a couple of millimeters in diameter. On top of the fine grained succession lies a ~2 m thick layer of coarse gravels to boulders that is capped by a thin layer of loess (Figure 17a).

We sampled the three fine-grained layers within the fluvial sequence at depths of 0.8 m, 0.95 m, and 1.7 m below the gravels, respectively (Figure 17a). The uppermost sample (chilik-2016-upper) was a bulk sample with some charcoal in it and returned an age of 15,360–15,075 cal years B.P. The samples from the middle layer (chilik-2016-middle) and from the lower layer (chilik-2016-lower) were pieces of charcoal and returned an age of 13,425–13,215 cal years B.P. and 13,735–13,115 cal years B.P., respectively. Our uppermost sample is older than the lower ones, which may be explained with reworking of the sediment before its final deposition at the current location. We have no direct constraints on possible inheritance of the samples, which would change the slip rates we calculate. However, we might expect that inheritance would not change our results substantially given the uncertainties and the age ranges of our samples. Since this is a bulk sample including fine-grained sediment, the age is likely somewhat overestimated. The gravel layer on top of the fine-grained material indicates rapid deposition. We conclude that the terrace surface was abandoned not earlier than ~15 ka ago and probably not much later than ~13.5 ka ago. In the following, we use an age range of 13.3–15 ka for our slip rate calculations.

4.3.1.3. Slip Rate

The age of terrace T2 and the corresponding measured vertical offset of ~14.5 m at the left bank of the river give an uplift rate of ~1–1.1 mm/a. The uncertainties in stratigraphic position of the samples and the error related to matching the footwall and the hanging wall across the fault do not justify calculating a more precise rate with propagating formal errors. We have no direct information on the dip of the fault; see discussion in section 5.1. A dip of 45° would result in a fault slip rate of ~1.4–1.6 mm/a. A shallower fault with a dip of only 30° would have a slip rate of 2–2.2 mm/a, and a fault with a dip of 60° would yield a slip rate of 1.2–1.3 mm/a. The lowest terrace we encountered at site S7 has a vertical offset of 14 m at the left bank of the river (Figure 16). This is much higher than the offsets observed elsewhere along the Almaty range front, for

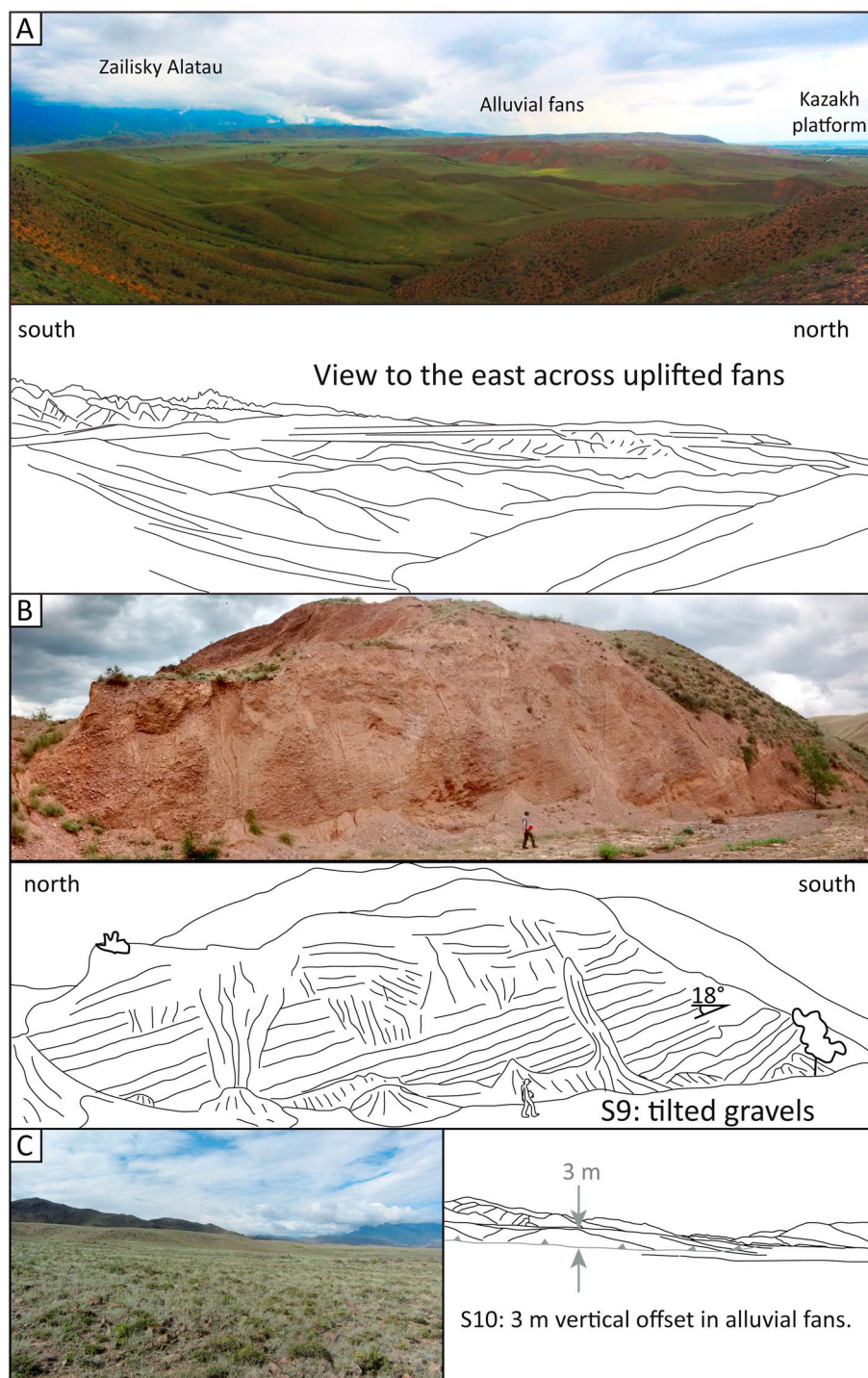


Figure 19. (a) Stacked field photo and sketch drawing of uplifted terraces in between the Zailisky Alatau rangefront and the Kazakh platform. (b) Field photo and sketch drawing of tilted gravel layers that crop out in a riverbank at site S9. The gravels dip 18° to the north and are bound to the north by a reverse fault. (c) Field photo and sketch drawing of the fault scarp at site S10 where we found alluvial fans with 3 m vertical offset. See Figure 13 for location.

example, at sites S1 and S2, and is also higher than the scarp found at Rahat (S6). The terrace has very likely been formed in multiple earthquake events. We conclude that the rangefront fault has a slip rate of between ~ 1.2 – 2.2 mm/a in this section, averaged over multiple earthquakes in the past ~ 13.3 – 15 ka and assuming dips of 30° – 60° .

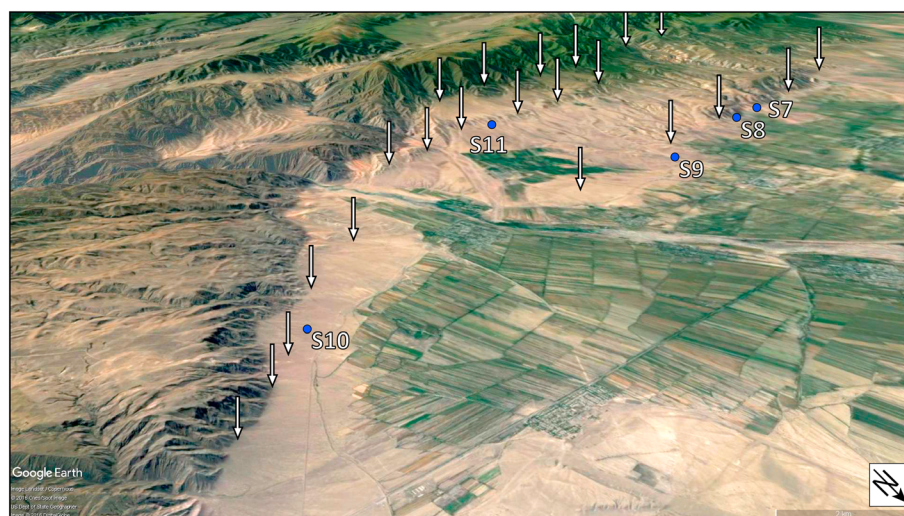


Figure 20. Oblique view to the southwest. Three distinct fault traces (white arrows) are visible in between the Kazakh platform and the Zailisky Alatau. The folded terraces in the center of the plateau near S11 and the fault in the north were investigated by Selander et al. (2012). Blue dots indicate the study sites S7–S11 in the eastern part of the Almaty rangefront fault. Imagery: GoogleEarth.

4.3.2. The Big Almaty Canal (S8)

The Big Almaty Canal (russ. Большой Алматинский канал; kaz. Үлкен Алматы каналы) is an irrigation canal that diverts water from the River Chilik further east to the Almaty metropolitan area where the water mainly serves agricultural and industrial needs. The canal was built in the late 1970s and contours around the front of the Zailisky Alatau for more than 150 km. From an engineering point of view, there are good reasons for choosing this location: the water is always available at an elevation higher than the crops, and close to the mountain front, the canal can maintain a constant slope without having to circumnavigate the numerous alluvial fans. At some locations, the canal crosses streams and roads coming from the mountains. These crossings were realized with underground sections, tunnels, and aqueducts. Since construction of the canal required massive excavations, large stretches of the mountain front, where we suspect the rangefront fault to crop out, are now covered either by spoil or by the canal itself. Knowledge on past surface ruptures along the canal would not only help to understand the tectonic behavior of the rangefront fault but also be interesting from a seismic risk and infrastructure vulnerability point of view.

We analyzed declassified Corona satellite imagery that was acquired in 1969 before the canal was built (Figure 18). Along the rangefront, we identified several spots in which fault scarps can clearly be seen in the grayscale satellite photos. Most of these locations can also be found in modern Google Earth imagery. We found that the canal crosses the rangefront fault scarp several times. At study site S8, the canal was built directly on the scarp (arrows in Figure 18) for a stretch a couple of hundred meters long. In this section the fault scarp appears as a very sharp line in smooth alluvial surfaces. Here it is much clearer in the imagery than in most other sites along the rangefront.

Unfortunately, the canal deprives us of the opportunity to study these scarps in more detail, but the Corona imagery makes clear that the mountain front has been tectonically active in the past. No direct age control is available for this section of the fault, but the sharp morphological expression of the rupture leads us to conclude that it might be Holocene in age. We made our analysis of the Corona imagery after our field visit; future fieldwork can aim to inspect the scarps in more detail and to evaluate their potential as paleoseismological trenching sites.

4.3.3. East of Chilik (S9, S10, and S11)

In the easternmost part of the Zailisky Alatau, a ~10 km wide plateau with an elevation of 1,100–1,600 m separates the Kazakh platform from the highest parts of the mountain range (Figure 13). The plateau is formed of folded alluvial surfaces; river cuts expose folded Cenozoic basin deposits. Abrupt breaks in slope mark both the northern and the southern boundaries of that plateau (Figure 13). Around 78°E, a second fault strand parallel to the mountain front and within the plateau becomes visible. This strand runs ~5 km S of the

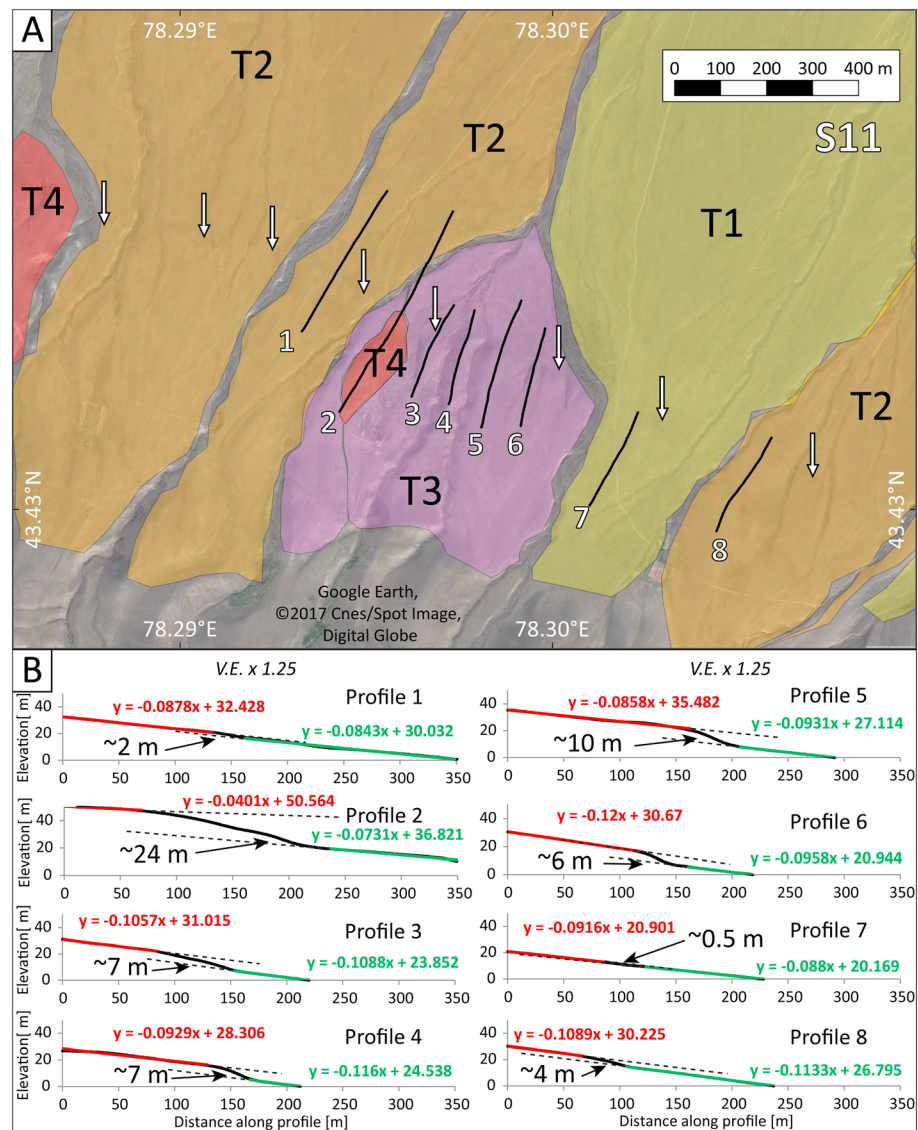


Figure 21. Study site S11. (a) Map showing the fault scarp (white arrows) and the four different fan levels T1–T4 (youngest–oldest) in Google Earth. Black lines are the eight DGPS profiles presented in Figure 21b. (b) Topographic profiles 1–8 (vertically exaggerated). Note that the elevation differences along profile rather than absolute elevations are plotted for comparability. Black number indicates vertical throw measured at the position marked by the black arrow in each profile. Profile 7 is located on T1, and profiles 1 and 8 measure the offset of fan T2. Alluvial fan T3 is probed by profiles 3–6, and profile 2 crosses the oldest fan T4.

piedmont and is mainly expressed as folded alluvial surfaces. Here Selander et al. (2012) estimated fault slip rates of 0.8 ± 0.5 mm/a and 0.43 ± 0.3 mm/a for the frontal fault and the fault within the plateau, respectively. These values are based on vertical offset measurements, and ages of 100 ± 30 ka are based on regional terrace correlation (cf. Thompson et al., 2002). We investigated three sites S9–S11 near Chilik (Figures 13, 19, and 20).

4.3.3.1. Site S9

At S9 we observe three parallel faults that offset alluvial fans (Figures 13 and 19). The composition of those alluvial fans and their stratigraphy are exposed in a riverbank at S9 where a small intermittent stream cuts into the scarp (Figure 19b). We find mainly medium to coarse gravels with a few finer-grained sandy units. The gravels are probably Pleistocene in age. In general, the layers are subparallel with a few exceptions of internally deformed gravels on a meter-scale. The fault itself does not crop out at S9. The general dip of the strata is 18° to the north. This dip is much steeper than that of active alluvial fans anywhere near the

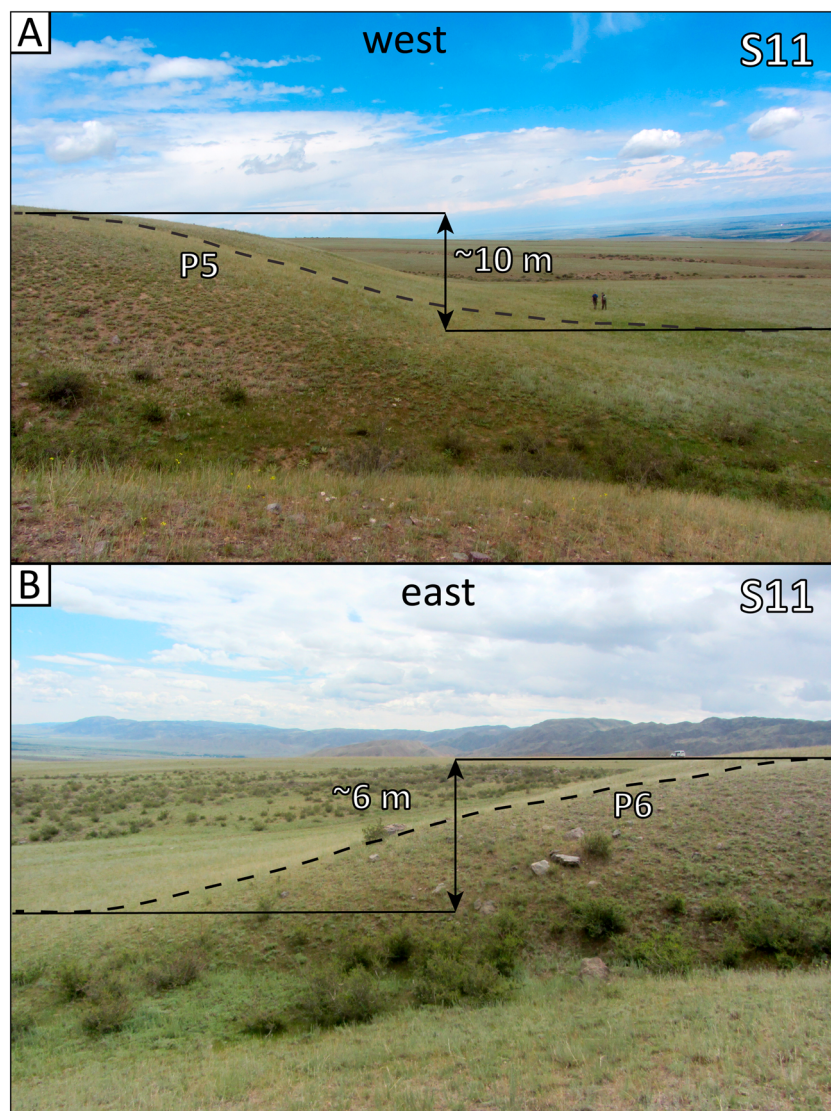


Figure 22. Fault scarps in fan T3 at site S11. (a) Photo looking west to profile P5. Here we measured ~10 m vertical offset with DGPS. Note the two geologists for scale. (b) Photo looking east to P6 with ~6 m of vertical offset. Both scarps probably record multiple earthquake events.

range front and also steeper than the alluvial surfaces further south. We interpret these findings as evidence for folding related to an underlying reverse fault, possibly a fault-propagation fold.

4.3.3.2. Site S10

Site S10 is situated at the mountain front ~12 km east of S9. A distinct fault scarp offsets alluvial fans up to 1 km north of the main range front. The scarp can be traced for more than 7.5 km and is expressed in different generations of alluvial fans (Figures 13 and 19c). Its height varies from less than 1 m to several meters in old fans. The scarp is degraded and expressed as zone of steepened slope several tens of meters wide. Here, at the eastern end of the Almaty range front fault, we estimated ~3 m of vertical offset in a section that may represent a single-event scarp (Figure 19c). We have no age control of the offset alluvial fans, but comparison with similar scarps elsewhere along the fault and in the vicinity indicates that it probably occurred after the LGM. The shape of the scarp also suggests that the last surface rupturing event did not occur in the very recent past.

4.3.3.3. Site S11

Site S11 is situated close to the Selander et al. (2012) study site (Figures 13 and 20). Here a fault scarp that separates different generations of alluvial fans is expressed in the center of the plateau between the high

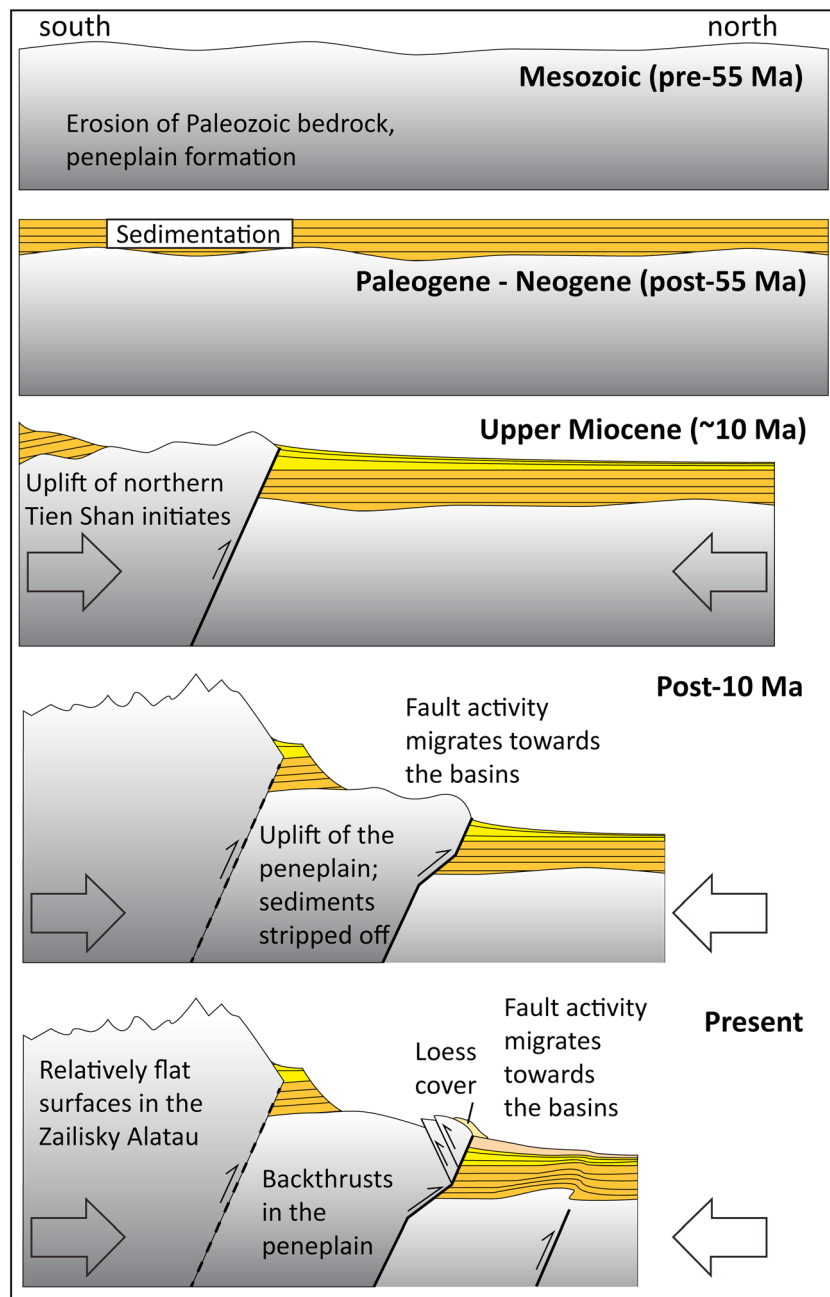


Figure 23. Generalized evolution of the Zailisky Alatau since the Mesozoic, not to scale. Solid lines mark active faults, while dashed lines mark faults that are at less active.

Zailisky Alatau and the Kazakh platform (Figures 20 and 21). The fans are incised by ephemeral channels as a result of recent uplift. We identified four different generations of fans T1–T4 (youngest–oldest) based on their morphology, cross-cutting relationships, degree of dissection, and elevation (Figure 21a). The fault scarp can be traced for approximately 10 km. All generations of fans are offset except the most recent river channels. The oldest fans show larger offsets than the younger ones (Figures 21a and 21b).

We measured the height of the scarp at eight locations using DGPS profiles and the methods described above (Figure 21a). Our profiles cover four different fan generations T1–T4 and therefore return scarp heights that vary depending on the number of earthquakes that offset the alluvial fans since their abandonment (Figure 21b).

The rather young and undissected fan surface T1 has an offset of only ~0.5 m (profile 7). This offset occurs south of the main scarp observed in neighboring fans and may indicate a secondary fault strand.

Surface T2 is also rather smooth and affected by little incision. Our measurements show a vertical offset of ~2 m in profile 1 and of ~4 m in profile 8.

Fan surface T3 is more intensely dissected and higher than T1 and T2. It covers a smaller area because it has been partly eroded by later fan generations. Profiles 3–6 show that T3 is vertically offset by ~6–10 m and has very likely recorded multiple events.

Profile 2 reveals a cumulative, degraded scarp that offsets the oldest surface T4 by ~24 m. No sharp break in slope is visible here; instead, the scarp is a zone more than 150 m wide. We interpret this as the result of repeated offset in surface rupturing earthquakes and subsequent erosion and degradation of the scarp.

Without further dating, we cannot distinguish whether T1 and T2 record a single earthquake only or multiple earthquakes. The larger offsets of 6–10 m in T3 likely indicate multiple events (Figure 22). Terrace T4, with its 24 m high composite scarp, is interpreted to have formed in even more earthquakes.

5. Discussion

Our survey revealed a variety of geomorphic evidence for post-LGM/Holocene faulting along the Almaty section of the Zailisky Alatau range front. We document thrust fault scarps at the range front and in alluvial fans (S1–S4, S6, and S8–11), uplifted river terraces (S7), deformed soft sediments and folding in the foreland (W–NW of Almaty and the Kosmos site of Macklin et al., 2015), folding along the range front (S5), and back-thrusts in the peneplain. We have shown that active deformation is not restricted to the immediate range front. Parallel fault strands are active in some places, and deformation also extends into the foreland and the peneplain. Ongoing loess sedimentation over the past few millions years complicates the assessment of both short-term and long-term differential tectonic uplift as the aggrading loess changes the surface elevations and erosional properties. However, 50–100 m high scarps are present along most of the range front. In the following, we discuss the implications for the occurrence of large earthquakes, local fault segmentation, fault slip rates, seismic hazard, and the evolution of the Northern Tien Shan.

5.1. Earthquake Magnitudes Along the Almaty Range front

The largest historical earthquake that occurred at or near the Almaty range front was the $M \sim 7.3$ Verny earthquake of 1887 (Hay, 1888; Mushketov, 1890; Tatevossian, 2007). We did not find any fault offsets that appeared fresh enough in terms of scarp morphology and preservation to be likely related to this event only 130 years ago (cf. Abdрахmatov et al., 2016; Arrowsmith et al., 2017; Grützner et al., 2017, for examples of scarp preservation in the area). Instead, at various sites along the range front, we observed degraded fault scarps in alluvial fans with heights of approximately 2–4 m. Paleoseismological trenching could determine if these scarps represent single-event scarps or cumulative offsets. However, we note that for almost all sites we did not find any smaller scarps although different generations of alluvial surfaces were recognized. This observation may be explained by a climate-driven event of fan formation, probably related to the end of the LGM. In this case we would see single or multiple earthquake scarps in fans of similar age. Another explanation would be that the scarps do indeed represent single-event offsets and that we do not observe smaller scarps because only the most recent event is preserved in the landscape, as is the case in the basin to the east of the Zailisky Alatau (Grützner et al., 2017). Given the rather long recurrence intervals of surface-breaking earthquakes in the Tien Shan (Abdрахmatov et al., 2016; Campbell et al., 2015; Landgraf et al., 2016; Thompson, 2001), the absence of smaller scarps, and the state of degradation, we consider it likely that at least some of the 2–4 m high features were formed in single events in the Holocene. Larger amounts of vertical offsets are observed at various sites, but in all those cases, the presence of nearby smaller scarps suggests that these scarps formed in multiple events.

If these vertical offsets were related to single event scarps, they would likely correspond to paleo-earthquakes exceeding $M_{6.8-7}$ (Wells & Coppersmith, 1994). However, recent large reverse faulting events showed a remarkable variability of surface displacement. For example, no significant surface ruptures occurred in the 2015 Gorkha earthquake despite being a magnitude of $M_w 7.8$ with an aftershock of $M_w 7.3$ (Lindsey et al., 2015; Wang & Fialko, 2015), with only centimeter-scale surface offsets observed on

a subsidiary fault splay instead (Elliott et al., 2016). However, this earthquake ruptured a very gently dipping fault plane of approximately 8° with a complex ramp and flat geometry. The 1992 Suusamyр earthquake struck in Kyrgyzstan (Western Tien Shan) with a magnitude of $M_{\text{S}}7.3$ on a much steeper dipping fault plane ($\sim 60^\circ$; Mellors et al., 1997). It produced a rather unusual surface rupture pattern at two sites more than 25 km apart. One segment recorded up to 2.7 m of vertical offset with an extent of not more than 500 m. The second set of ruptures was more than 3 km long but showed much less than 2 m of vertical offset (Bogachkin et al., 1997; Ghose et al., 1997). The two examples of Gorkha and Suusamyр and the observations from the 1887 Verny earthquake illustrate that determining earthquake magnitudes from surface offsets may be of limited use in tectonic settings such as the Tien Shan. However, a 2–4 m high fault scarp certainly indicates a strong earthquake. Our estimate of $M > 6.8$ for the scarps that we investigated must therefore be taken as a minimum value.

Instead of using surface offsets, information on magnitudes could be derived from the lengths of surface breaks. We found scarps of possible post-LGM age along the entire Almaty range front. Our observations cover a distance of more than 250 km along strike (Figure 2). Empirical scaling relationships suggest a magnitude of ~ 8 for an earthquake with such a rupture length. Similar magnitudes and rupture lengths were reported for the 1889 Chilik earthquake (Abdrakhmatov et al., 2016; Krüger et al., 2015) and the 1911 Chon Kemin event (Arrowsmith et al., 2017; Delvaux et al., 2001; Kulikova & Krüger, 2015). However, the surface offsets both in 1889 and 1911 were much greater than ~ 3 m. We found the distribution of possible single-event fault scarps along the range front to be scattered and, over large reaches, obscured by anthropogenic landscape modification. It is therefore not possible to identify potential sections marked by shorter, continuous scarps. This hampers any further speculation on surface rupture length versus magnitude relations, and we have no evidence that the range front fault ruptured in its entire length in one event.

We also observe that the fault traces along the range front overlap and that individual fault strands and folds do not seem to exceed ~ 100 km in length. This may be interpreted as segmentation of the range front fault, which would mean that a rupture of the entire fault is somewhat less likely than smaller earthquakes involving only parts of the range front. However, recent large earthquakes show that multiple faults can rupture in one event (e.g., Tabas, Iran (Berberian, 1979; Walker et al., 2003) and Kaikoura, New Zealand (Hamling et al., 2017)), and earthquakes may rupture multiple faults despite being separated by several kilometers (Abdrakhmatov et al., 2016; Nissen et al., 2016; Wesnousky, 2006, 2008). We have no dating results that would support a single earthquake as the cause for all the possible single-event fault scarps that we observed. The pattern can also be explained with multiple smaller earthquakes along the Zailisky Alatau. This would imply that the range front does not necessarily release the accumulated stress along its entire length in a single large earthquake. Our study did not reveal systematic variations in the state of degradation of the fault scarps that would be evidence for multiple distinct ruptures. The lack of scarps along some sections of the range front could either be explained with blind faulting, inactivity since the LGM or in the Holocene, or partial erosion. Recent studies have, however, shown that faults in the Tien Shan tend to break in rare but exceptionally large events (Campbell et al., 2013, 2015; Deng et al., 1996; Grützner et al., 2017; Korjenkov et al., 2011). We conclude that the Almaty range front has been hit by surface rupturing earthquakes of $M > 6.8$ and probably much stronger in the recent past.

5.2. Paleo-Earthquake Timing

We do not have direct age measurements from the offset morphological markers except at site S7, but our observations allow us to place constraints on the timing of the last surface rupturing earthquakes. The 2–4 m high scarps offset alluvial fan surfaces that are only minimally incised. Those fan surfaces probably correlate with a post-LGM terrace (10–15 ka) observed in the Kyrgyz Tien Shan (Korjenkov et al., 2002, 2007; Landgraf et al., 2016; Thompson et al., 2002). Rapid fan accumulation post-LGM is also reported from the Chinese Tien Shan (e.g., Avouac et al., 1993). Grützner et al. (2017) found that fault scarps at the nearby Toraigyr Fault were obliterated by erosion between 3.6 ka and ~ 17 –40 ka. Fitzsimmons et al. (2016) document the deposition of significant amounts of loess along the Zailisky Alatau in the Holocene. These studies imply that it is unlikely for such a large number of rather small fault scarps to have survived if they were pre-Holocene. We suggest that probably all offsets of 2–3 m height that we document here are post-LGM and likely Holocene in age. The occurrence of well-preserved multi-event scarps and the dating at site S7 further indicate that not only one but several surface-rupturing earthquakes happened in the Holocene.

5.3. Seismic Hazard and Environmental Effects

The 1887 Verny earthquake demonstrated that one type of threat for Almaty comes from local faults that are right beneath or in the close vicinity of the city. Even if seismogenic structures could not produce an earthquake exceeding $M7.3$, they pose a significant hazard in terms of strong ground motion within the city limits. Earthquake environmental effects, like landslides, and cascading effects, like unstable landslide-dammed lakes, are an additional concern in the rugged topography and thick loess deposits underlying the growing outskirts of the city. Major landslides were documented in the steep loess hills in 1887 (Mushketov, 1890; Tatevossian, 2007). Those hills are now a major concern since they were subject to urban development in the very recent past (Figure 20). A surface-rupturing earthquake beneath Almaty, such as the ones that we have detected as surface offsets in the alluvial fans, would likely result in a large number of slope failures that affect now densely populated areas (Figures 21a and 21b).

Our study shows that in contrast to what was learned from 1887, not only shaking but also surface faulting must be taken into account. The effects of surface offset are somewhat different from shaking in that such ruptures will cut utilities and crucial lifelines, block roads, and damage critical infrastructure built on top. The Big Almaty Canal, for example, crosses the range-front fault several times and is, in significant parts, built directly on top of the Holocene scarps. We point out that a future surface rupturing earthquake might severely damage the canal with dire consequences for Almaty and for the settlements near the breach.

The two earthquakes that damaged Almaty in 1889 and 1911 happened far away from the city but, due to their large magnitudes, caused devastating shaking in the city. A similar effect can be expected from structures that we found to be active further away from Almaty. We have shown that the entire area west and northwest of the city undergoes differential uplift, recorded by the drainage pattern. This uplift might happen above blind faults in the Kazakh platform whose lengths and offsets are entirely unknown. Post-LGM folding as far north as Kosmos provides information on the scale of these structures. Also, in large parts of the range-front, we observed more than one active fault strand. It is unknown whether or not they can rupture together with other strands or whether this happened in the past.

The fact that all the scarps that we found show strong degradation indicates that the last surface ruptures occurred a relatively long time, probably thousands of years, ago. If all the accumulated strain is released seismically and if the seismic cycle model can be applied to the Almaty range-front (cf. Liu & Stein, 2016), this may mean that the faults are loaded for thousands of years and that they are in a late stage of their cycle.

5.4. Evolution of the Zailisky Alatau

Our observations allow us to make some final remarks on the evolution of the Zailisky Alatau as a result of the far-field compressive stress caused by the collision of India and Eurasia. The uplifted Mesozoic peneplain (Figure 2) not only is a well-preserved marker at intermediate elevations but also controls the morphology of the highest parts of the range that are characterized by a remarkably flat top (Figures 1b, 2a, and 4c). This is probably evidence for relatively fast uplift, because otherwise the highest parts of the range would be more thoroughly eroded by the large rivers draining the Tien Shan. Our observations further indicate that at the onset of uplift in the Northern Tien Shan in the Upper Miocene, the active fault lay between the high Zailisky Alatau and the now uplifted peneplain (Figure 23). The lack of Cenozoic sediments in the higher parts of the mountains may suggest that erosion was greatest in the most rapidly growing areas of the mountains and first stripped off most of the Paleogene and Neogene sedimentary cover. With sedimentary cover stripped, then the steep valleys in which rivers drain the mountain range today were carved into the underlying uplifted bedrock. However, it is not well resolved how thick the Cenozoic cover was and if it existed everywhere in the Northern Tien Shan.

The majority of our observations concern the Almaty range-front fault. We show that this range is the most active structure of the Northern Tien Shan boundary today. The uplift of the peneplain to an intermediate elevation by this fault shows that fault activity then migrated toward the Kazakh platform, and a new fault formed or an inherited structure was reactivated. Consequently, another sector of the peneplain was uplifted. Further incision into the bedrock has created several steep canyons, but overall, the old erosional surface is well preserved and a reliable marker of differential uplift.

Finally, we observe that the most recent generation of faults affects the Kazakh platform north of the mountain front. Evidence for this is found in soft-sediment deformation, local uplift, and folding. Again, we observe

the basinward migration of fault activity. This uplift is at least partly related to blind faults that do not yet reach the surface. The backthrusts at the edge of the peneplain probably also formed relatively recently as they are prominent and not dissected. Backthrusts are usually associated with a change of fault dip at depth. In a ramp geometry, the fault steepens near the surface, leading to a space problem above that zone. Backthrusting is a way to accommodate the additional space by expelling a wedge of material (Figure 23; Erickson, 1995).

Despite the evidence for active tectonics in the Kazakh platform, the range front fault is still active, as recorded by the Holocene fault scarps. This is a feature that we observed all along the northern part of the Zailisky Alatau. Active deformation is not restricted to a single fault but often distributed among a series of parallel structures. A similar observation was made for sets of normal faults in Greece (Goldsworthy & Jackson, 2001): although fault activity migrates toward the basin, the other more mature faults still show some level of activity. The propagation of active faulting toward the basins has been explained by applying the critical taper theory to accretionary wedges (Davis et al., 1983). Similarly, Dahlen et al. (1984) used cohesive coulomb criteria to explain the mechanics of the propagation of the fold-and-thrust belt in western Taiwan. Our observations indicate that a similar mechanism may apply to the Northern Tien Shan. Thompson et al. (2002) show that the deformation is not concentrated along the frontal fault of the Kyrgyz Tien Shan but occurs across a number of distributed active structures. This is in agreement with geological observations from the Southern Tien Shan (Thompson Jobe et al., 2017) and other mountain ranges (Boyer, 1992), analogue modeling (Koyi et al., 2000), numerical experiments (Willett, 1999), GPS data from Central Asia (Zubovich et al., 2010), and instrumental earthquakes throughout the Tien Shan (Sloan et al., 2011).

The fate of the Kazakh platform north of Almaty is that of the peneplain: uplift will continue and erosion will strip off the Paleogene–Recent sediments on which Almaty is built, and a new peneplain bedrock surface will form. What is now the peneplain will become more intensely incised and further uplifted such that the clear morphological difference between the high Zailisky Alatau and the peneplain will decline.

6. Conclusions

We have shown that the Almaty range front has had surface-rupturing earthquakes in the Holocene and that active deformation can be found all along the northern front of the Zailisky Alatau. The record of tectonic shortening in the landscape encompasses fault scarps possibly from single and multiple events in alluvial fans, folding, uplifted abandoned river terraces, and backthrusts. We observe active structures not only at the main topographic step along the foothills but also in the platform and in the mountains. The area west and north of Almaty experiences uplift, and the city itself is located on the hanging wall of blind thrust fold deforming the foreland. We estimate that earthquakes of at least $M > 6.8$ –7 are necessary to produce the observed scarps if they resulted from single events. The 1887 Verny earthquake did not rupture the surface as far as we know, which may imply that the surface ruptures that we found stem from stronger events ($M > 7.3$). The state of scarp degradation implies that the causative earthquakes happened relatively long ago. This may have implications for seismic hazard, as the elapsed time since the last earthquake might be considered an indicator for ongoing strain accumulation that brings the faults closer to failure. Quaternary dating of an uplifted river terrace east of Almaty allowed us to determine a Holocene uplift rate of 1–1.1 mm/a, which corresponds to a fault slip rate of about 1.2–2.2 mm/a depending upon the fault dip. This is the first slip rate measured along the range front and represents not more than a quarter of the total shortening rate between Lake Issyk Kul and the Kazakh platform. Although the Zailisky Alatau has such impressive morphology, the slip rate is not extraordinarily high and is comparable to faults further west in Kyrgyzstan (Thompson et al., 2002). We show that the active faults pose a significant threat to Almaty since the city is built directly on top of the currently deforming structures. The fact that the geomorphic evidence for active faulting and folding has not been reported from the Almaty range front is partly due to the rather subtle geomorphological expression of active deformation, for example, in Almaty and near Talgar. Other obstructions include the thick loess cover that blankets the foothills and partly obscures evidence of large ancient earthquakes and the anthropogenic obliteration of fault scarps. High-resolution topographic data can, however, overcome these problems in many places. We emphasize the usefulness of employing high-resolution topography data such as stereo-satellite imagery, drone-based DEMs, and DGPS surveying.

Acknowledgments

This research was run under the Earthquakes without Frontiers project, funded by NERC and ESRC (grant code: EwF_NE/J02001X/1_1), and within the Centre for Observation and Modelling of Earthquakes and Tectonics (COMET). SPOT imagery was acquired with a grant from EwF. The ALOS Global Digital Surface Model (AW3D30) is provided by and is copyright of JAXA. Corona and SRTM data are distributed by the Land Processes Distributed Active Archive Center (LP DAAC), located at USGS/EROS, Sioux Falls, SD, <http://lpdaac.usgs.gov>. The drone DEMs will be made available through OpenTopography (www.opentopography.org). J.R.E. is funded as a Royal Society University Research Fellow. We thank Barry Parsons, Kathryn Fitzsimmons, and Tobi Sprafke for help and discussions in the field. Jessica Thompson Jobe, an anonymous reviewer, and the Editor Taylor Schildgen provided valuable comments that helped to significantly improve the manuscript. Figure 1 was prepared with the Generic Mapping Tool software by Wessel and Smith (1998).

References

- Abdrakhmatov, K., Walker, R. T., Campbell, G. E., Carr, A. S., Elliott, A., Hillemann, C., ... Sloan, R. A. (2016). Multi-segment rupture in the July 11th 1889 Chilik earthquake (M_w 8.0–8.3), Kazakh Tien Shan, identified from remote-sensing, field survey, and palaeoseismic trenching. *Journal of Geophysical Research: Solid Earth*, 121, 4615–4640. <https://doi.org/10.1002/2015JB012763>
- Abdrakhmatov, K., Weldon, R. J., Thompson, S. C., Burbank, D. W., Rubin, C., Miller, M., & Molnar, P. (2001). Onset, style and current rate of shortening in the central Tien Shan, Kyrgyz Republic. *Russian Geology and Geophysics*, 42(10), 1585–1609.
- Abdrakhmatov, K. Y., Aldazhanov, S. A., Hager, B. H., Hamburger, M. W., Herring, T. A., Kalabaev, K. B., ... Zubovich, A. V. (1996). Relatively recent construction of the Tien Shan inferred from GPS measurements of present-day crustal deformation rates. *Nature*, 384(6608), 450–453. <https://doi.org/10.1038/384450a0>
- Abdrakhmatov, K. Y., Djanuzakov, K. D., & Delvaux, D. (2002). Active tectonics and seismic hazard of the Issyk-Kul basin in the Kyrgyz Tian-Shan. *Lake Issyk-Kul: Its Natural Environment*, 13, 147–160.
- Arrowsmith, J. R., Crosby, C. J., Korzhnikov, A. M., Mamyrov, E., Povolotskaya, I., Guralnik, B., & Landgraf, A. (2017). Surface rupture of the 1911 Kebin (Chon-Kemin) earthquake, northern Tien Shan, Kyrgyzstan. *Geological Society, London, Special Publications*, 432(1), 233–253.
- Atrushkevitch, P. A., Kalabaev, N. B., Kartashov, A. P., Lototsky, V. D., & Ostropico, P. A. (1988). Research on crustal movements on the Alma-Ata polygon, northern Tien Shan. *Journal of Geodynamics*, 9(2–4), 279–292.
- Avouac, J. P., Tapponnier, P., Bai, M., You, H., & Wang, G. (1993). Active thrusting and folding along the northern Tien Shan and Late Cenozoic rotation of the Tarim relative to Dzungaria and Kazakhstan. *Journal of Geophysical Research*, 98(B4), 6755–6804. <https://doi.org/10.1029/92JB01963>
- Bemis, S. P., Mickelthwaite, S., Turner, D., James, M. R., Akciz, S., Thiele, S. T., & Bangash, H. A. (2014). Ground-based and UAV-based photogrammetry: A multi-scale, high-resolution mapping tool for structural geology and paleoseismology. *Journal of Structural Geology*, 69, 163–178.
- Berberian, M. (1979). Earthquake faulting and bedding thrust associated with the Tabas-e-Golshan (Iran) earthquake of September 16, 1978. *Bulletin of the Seismological Society of America*, 69(6), 1861–1887.
- Bindi, D., Parolai, S., Gómez-Capera, A., Locati, M., Kalmetyeva, Z., & Mikhailova, N. (2014). Locations and magnitudes of earthquakes in Central Asia from seismic intensity data. *Journal of Seismology*, 18(1), 1–21. <https://doi.org/10.1007/s10950-013-9392-1>
- Bogachkin, B. M., Korzhnikov, A. M., Mamyrov, E., Nechaev, Y. V., Omuraliev, M., Petrosyan, A. E., ... Charimov, T. A. (1997). The structure of the 1992 Susamyr earthquake source based on its geological and seismological manifestations. *Izvestiya Physics of the Solid Earth*, 33(11), 867–882.
- Bogdanovich, K. I., Kark, I. M., Korolkov, B. Y., & Mushketov, D. I. (1914). *Earthquake in northern district of Tien Shan, 22 December 1910 (4 January 1911)*. Leningrad in Russian: Commission of the Geology Committee.
- Bowman, D., Korjenkov, A., Porat, N., & Czassny, B. (2004). Morphological response to Quaternary deformation at an intermontane basin piedmont, the northern Tien Shan, Kyrgyzstan. *Geomorphology*, 63(1–2), 1–24.
- Boyer, S. E. (1992). Geometric evidence for synchronous thrusting in the southern Alberta and northwest Montana thrust belts. In K. R. McClay (Ed.), *Thrust tectonics* (pp. 377–390). New York: Chapman and Hall.
- Brown, E. T., Bourlés, D. L., Burchfiel, B. C., Qidong, D., Jun, L., Molnar, P., ... Yiu, F. (1998). Estimation of slip rates in the southern Tien Shan using cosmic ray exposure dates of abandoned alluvial fans. *Geological Society of America Bulletin*, 110(3), 377–386. [https://doi.org/10.1130/0016-7606\(1998\)110<0377:EOSRIT>2.3.CO;2](https://doi.org/10.1130/0016-7606(1998)110<0377:EOSRIT>2.3.CO;2)
- Bull, W., & McFadden, L. (1977). Tectonic geomorphology north and south of the Garlock fault, California. In D. E. Doehring (Ed.), *Geomorphology in arid regions, Proceedings 8th Annual Geomorphology Symposium* (pp. 115–137). Binghamton: State University of New York.
- Bullen, M. E., Burbank, D. W., & Garver, J. I. (2003). Building the northern Tien Shan: Integrated thermal, structural, and topographic constraints. *The Journal of Geology*, 111(2), 149–165.
- Burbank, D. W., McLean, J. K., Bullen, M., Abdrakhmatov, K. Y., & Miller, M. M. (1999). Partitioning of intermontane basins by thrust-related folding, Tien Shan, Kyrgyzstan. *Basin Research*, 11(1), 75–92.
- Burgette, R. J., Weldon, R. J., Abdrakhmatov, K. Y., Ormukov, C., Owen, L. A., & Thompson, S. C. (2017). Timing and process of river and lake terrace formation in the Kyrgyz Tien Shan. *Quaternary Science Reviews*, 159, 15–34.
- Burtman, V. S. (1975). Structural geology of Variscan Tien Shan, USSR. *American Journal of Science*, 275-a, 157–186.
- Buslov, M. M., Kokh, D. A., & De Grave, J. (2008). Mesozoic–Cenozoic tectonics and geodynamics of Altai, Tien Shan, and northern Kazakhstan, from apatite fission-track data. *Russian Geology and Geophysics*, 49(9), 648–654.
- Campbell, G. E., Walker, R. T., Abdrakhmatov, K., Jackson, J. A., Elliott, J. R., Mackenzie, D., ... Schwenninger, J. L. (2015). Great earthquakes in low strain rate continental interiors: An example from SE Kazakhstan. *Journal of Geophysical Research: Solid Earth*, 120, 5507–5534. <https://doi.org/10.1002/2015JB011925>
- Campbell, G. E., Walker, R. T., Abdrakhmatov, K., Schwenninger, J. L., Jackson, J. A., Elliott, J. R., & Copley, A. C. (2013). The Dzhungarian fault: Late Quaternary tectonics and slip rate of a major right-lateral strike-slip fault in the northern Tien Shan region. *Journal of Geophysical Research: Solid Earth*, 118, 5681–5698. <https://doi.org/10.1002/jgrb.50367>
- Clark, P. U., Dyke, A. S., Shakun, J. D., Carlson, A. E., Clark, J., Wohlfarth, B., ... McCabe, A. M. (2009). The last glacial maximum. *Science*, 325(5941), 710–714.
- CMT (2016). Global centroid–moment–tensor (CMT) catalog. CMT catalog web search. Retrieved from <http://www.globalcmt.org/CMTsearch.html>. Last access 25 December 2016.
- Crosby, C. J., Arrowsmith, J. R., Korjenkov, A. M., Guralnik, B., Mamyrov, E., & Povolotskaya, I. E. (2007). *The hunt for surface rupture from the 1889 M_s 8.3 Chilik earthquake, northern Tien Shan, Kyrgyzstan and Kazakhstan*. Abstract T23D-1635 Presented at the 2007 AGU Fall Meeting, San Francisco, CA, Dec.
- Cuenca, M. C., Hooper, A. J., & Hanssen, R. F. (2013). Surface deformation induced by water influx in the abandoned coal mines in Limburg, The Netherlands observed by satellite radar interferometry. *Journal of Applied Geophysics*, 88, 1–11.
- Dahlen, F. A., Suppe, J., & Davis, D. (1984). Mechanics of fold-and-thrust belts and accretionary wedges: Cohesive Coulomb theory. *Journal of Geophysical Research*, 89(B12), 10,087–10,101. <https://doi.org/10.1029/JB089iB12p10087>
- Davis, D., Suppe, J., & Dahlen, F. A. (1983). Mechanics of fold-and-thrust belts and accretionary wedges. *Journal of Geophysical Research*, 88(B2), 1153–1172. <https://doi.org/10.1029/JB088iB02p01153>
- Delvaux, D., Abdrakhmatov, K. E., Lemzin, I. N., & Strom, A. L. (2001). Landslide and surface breaks of the 1911 M 8.2 Kemin earthquake. *Landslides*, 42(10), 1583–1592.
- Deng, Q., Zhang, P., Xu, X., Yang, X., Peng, S., & Feng, X. (1996). Paleoseismology of the northern piedmont of Tianshan Mountains, northwestern China. *Journal of Geophysical Research*, 101(B3), 5895–5920. <https://doi.org/10.1029/95JB02739>

- Elliott, J. R., Jolivet, R., Gonzalez, P., Avouac, J.-P., Hollingsworth, J., Searle, M., & Stevens, V. (2016). Himalayan megathrust geometry and relation to topography revealed by the Gorkha earthquake. *Nature Geoscience*, 9(2), 174–180. <https://doi.org/10.1038/NGEO2623>
- Engdahl, E., Van Der Hilst, R., & Buland, R. (1998). Global teleseismic earthquake relocation with improved travel times and procedures for depth determination. *Bulletin of the Seismological Society of America*, 88(3), 722–743.
- England, P., & Molnar, P. (2015). Rheology of the lithosphere beneath the central and western Tien Shan. *Journal of Geophysical Research: Solid Earth*, 120, 3803–3823. <https://doi.org/10.1002/2014JB011733>
- Erickson, S. G. (1995). Mechanics of triangle zones and passive-roof duplexes: Implications of finite-element models. *Tectonophysics*, 245(1–2), 1–11.
- Fitzsimmons, K. E., Sprafke, T., Zielhofer, C., Günter, C., Deom, J. M., Sala, R., & Iovita, R. (2016). Loess accumulation in the Tian Shan piedmont: Implications for palaeoenvironmental change in arid Central Asia. *Quaternary International*. <https://doi.org/10.1016/j.quaint.2016.07.041>
- Ghose, S., Mellors, R. J., Korjenkov, A. M., Hamburger, M. W., Pavlis, T. L., Pavlis, G. L., ... Muraliev, A. R. (1997). The $M_s = 7.3$ 1992 Suusamy, Kyrgyzstan, earthquake in the Tien Shan: 2. Aftershock focal mechanisms and surface deformation. *Bulletin of the Seismological Society of America*, 87(1), 23–38.
- Goldsworthy, M., & Jackson, J. (2001). Migration of activity within normal fault systems: Examples from the Quaternary of mainland Greece. *Journal of Structural Geology*, 23(2–3), 489–506.
- Gorshkov, G. P. (1947). *Tectonic earthquakes and seismic zonation of the territory of the USSR*. Russian: Foundation IFS AN USSR.
- Goryachev, A. V. (1959). *Mesozoic–Cenozoic structure, history, tectonic development, and seismicity of the regions of the Lake Issyk-Kul*. Moscow Russian: Academy of Sciences Publishing House.
- Grützner, C., Carson, E., Walker, R. T., Rhodes, E. J., Mukambayev, A., Mackenzie, D., ... Abdrakhmatov, K. (2017). Assessing the activity of faults in continental interiors: Palaeoseismic insights from SE Kazakhstan. *Earth and Planetary Science Letters*, 459, 93–104.
- Hall, M. E. (1997). Towards an absolute chronology for the Iron Age of Inner Asia. *Antiquity*, 71(274), 863–874.
- Hamling, I. J., Hreinsdóttir, S., Clark, K., Elliott, J., Liang, C., Fielding, E., ... Stirling, M. (2017). Complex multifault rupture during the 2016 M_w 7.8 Kaikōura earthquake, New Zealand. *Science*, 356(6334), eaam7194.
- Hay, M. B. (1888). The earthquakes of May and June, 1887, in the Verny (Vernoe) District, Russian Turkestan, and their consequences. *Proceedings of the Royal Geographical Society and Monthly Record of Geography*, 10(10), 638–646.
- ISC (2016). *International Seismological Centre, on-line catalog*. Thatcham, UK: International Seismological Centre. Retrieved from <http://www.isc.ac.uk>. Last access 12 December 2016
- Kondorskaya, N., & Shebalin, N. (1977). New catalog of strong earthquakes in the territory of the USSR from ancient times to 1975, Academy of Sciences, Moscow (English translation, updated through 1977, available as Report SE-31, World Data Center A for Solid Earth Geophysics, Boulder, CO, 606 pp.
- Koppes, M., Gillespie, A. R., Burke, R. M., Thompson, S. C., & Stone, J. (2008). Late Quaternary glaciation in the Kyrgyz Tien Shan. *Quaternary Science Reviews*, 27(7–8), 846–866.
- Korjenkov, A. M., Abdieva, S. V., Vakhrameeva, P. S., Dzhumabaeva, A. B., Mamyrov, E., Morozova, E. A., Orlova, L. A., & Fortuna, A. B. (2011). Strong historical earthquakes in the northwestern Issyk Kul' basin (northern Tien Shan). *Russian Geology and Geophysics*, 52(9), 955–962.
- Korjenkov, A. M., Arrowsmith, J. R., Crosby, C., Mamyrov, E., Orlova, L. A., Povolotskaya, I. E., & Tabaldiev, K. (2006). Seismogenic destruction of the Kamenka medieval fortress, northern Issyk-Kul region, Tien Shan (Kyrgyzstan). *Journal of Seismology*, 10(4), 431–442.
- Korjenkov, A. M., Kovalenko, V. A., & Usmanov, S. F. (2002). Long-term preservation of Paleoseismic deformation as a tool for revealing traces of ancient seismic catastrophes (example of the Chon-Kemin Valley, Kyrgyzstan). *Kartographische Bausteine*, 28, 137–154.
- Korjenkov, A. M., Povolotskaya, I. E., & Mamyrov, E. (2007). Morphologic expression of Quaternary deformation in the northwestern foothills of the Ysyk-Köl basin, Tien Shan. *Geotectonics*, 41(2), 130–148.
- Koyi, H. A., Hessami, K., & Teixell, A. (2000). Epicenter distribution and magnitude of earthquakes in fold-thrust belts: Insights from sandbox models. *Geophysical Research Letters*, 27(2), 273–276. <https://doi.org/10.1029/1999GL010833>
- Krüger, F., Kulikova, G., & Landgraf, A. (2015). Instrumental magnitude constraints for the 11 July 1889, Chilik earthquake. *Geological Society, London, Special Publications*, 432(1), 41–72.
- Kulikova, G., & Krüger, F. (2015). Source process of the 1911 $M_{8.0}$ Chon-Kemin earthquake: Investigation results by analogue seismic records. *Geophysical Journal International*, 201(3), 1891–1911.
- Landgraf, A., Dzhumabaeva, A., Abdrakhmatov, K. E., Strecker, M. R., Macaulay, E. A., Arrowsmith, J. R., ... Merchel, S. (2016). Repeated large-magnitude earthquakes in a tectonically active, low-strain continental interior: The northern Tien Shan, Kyrgyzstan. *Journal of Geophysical Research: Solid Earth*, 121, 3888–3910. <https://doi.org/10.1002/2015JB012714>
- Lindsey, E. O., Natsuaki, R., Xu, X., Shimada, M., Hashimoto, M., Melgar, D., & Sandwell, D. T. (2015). Line-of-sight displacement from ALOS-2 interferometry: M_w 7.8 Gorkha earthquake and M_w 7.3 aftershock. *Geophysical Research Letters*, 42, 6655–6661. <https://doi.org/10.1002/2015GL065385>
- Liu, M., & Stein, S. (2016). Mid-continental earthquakes: Spatiotemporal occurrences, causes, and hazards. *Earth-Science Reviews*, 162, 364–386.
- Machalett, B., Frechen, M., Hambach, U., Oches, E. A., Zöller, L., & Markovic, S. B. (2006). The loess sequence from Remisowka (northern boundary of the Tien Shan Mountains, Kazakhstan)—Part I: Luminescence dating. *Quaternary International*, 152–153, 192–201.
- Mackenzie, D., & Elliott, A. J. (2017). Untangling tectonic slip from the potentially misleading effects of landform geometry. *Geosphere*, 13(4). <https://doi.org/10.1130/GES01386.1>
- Mackenzie, D., Elliott, J. R., Altunel, E., Walker, R. T., Kurban, Y. C., Schwenninger, J. L., & Parsons, B. (2016). Seismotectonics and rupture process of the M_w 7.1 2011 Van reverse faulting earthquake, eastern Turkey, and implications for hazard in regions of distributed shortening. *Geophysical Journal International*, 206(1), 501–524. <https://doi.org/10.1093/gji/ggw158>
- Macklin, M. G., Panyushkina, I. P., Toonen, W. H., Chang, C., Tourtellotte, P. A., Duller, G. A., ... Prins, M. A. (2015). The influence of Late Pleistocene geomorphological inheritance and Holocene hydromorphic regimes on floodwater farming in the Talgar catchment, southeast Kazakhstan, Central Asia. *Quaternary Science Reviews*, 129, 85–95.
- Makarov, V. I. (1977). *New tectonic structures of the Central Tien Shan* (p. 171) (in Russian). Moscow: Order of the Red Banner Geology Institute, Akad. Sci.
- Mellors, R. J., Vernon, F. L., Pavlis, G. L., Abers, G. A., Hamburger, M. W., Ghose, S., & Iliassov, B. (1997). The $M_s = 7.3$ 1992 Suusamy, Kyrgyzstan, earthquake: Constraints on fault geometry and source parameters based on aftershocks and body-wave modeling. *Bulletin of the Seismological Society of America*, 87(1), 11–22.
- Mikhailova, N. N., Sokolova, I. N., Velikanov, A. Y., & Sokolov, A. N. (2015). Earthquakes on the territory of Almaty. *Vestnyk NYAC RK*, 3, 87–93.
- Mushketov, I. V. (1890). Le tremblement de terre de Verny, 28 Mai (9 Juin) 1887. *Memoires du Comite Geologique*, X(1), 65.

- Mushketov, I. V., & Orlov, A. P. (1893). Catalogue of earthquakes in the Russian empire (in Russian). *Zap. RGO*, 26, 582.
- Nalivkin, D. V. (1983). *Geological map of the USSR and adjoining water-covered areas* (scale 1:2,500,000). Leningrad: Ministry of Geology of the USSR, Karpinsky All-Union Order of Lenin Geological Research Institute.
- Nissen, E., Elliott, J. R., Sloan, R. A., Craig, T. J., Funning, G. J., Hutko, A., ... Wright, T. J. (2016). Limitations of rupture forecasting exposed by instantaneously triggered earthquake doublet. *Nature Geoscience*, 9(4), 330–336.
- Oskin, M. E., & Burbank, D. (2007). Transient landscape evolution of basement-cored uplifts: Example of the Kyrgyz range, Tian Shan. *Journal of Geophysical Research*, 112, F03S03. <https://doi.org/10.1029/2006JF000563>
- QGIS Development Team (2017). *QGIS geographic information system*. Open Source Geospatial Foundation Project. Retrieved from <http://www.qgis.org/>
- Reimer, P. J., Bard, E., Bayliss, A., Beck, J. W., Blackwell, P. G., Bronk Ramsey, C., ... van der Plicht, J. (2013). Int-Cal13 and Marine13 radiocarbon age calibration curves 0–50,000 years cal BP. *Radiocarbon*, 55(04), 1869–1887. <https://doi.org/10.1017/S0033822200048864>
- Riley, S. J., DeGloria, S. D., & Elliot, R. (1999). A terrain ruggedness index that quantifies topographic heterogeneity. *Intermountain Journal of Sciences*, 5, 23–27.
- Sala, R., & Deom, J. M. (2005). *Petroglyphs of South Kazakhstan* (p. 150). Almaty, Kazakhstan: Laboratory of Geoarchaeology.
- Selander, J., Oskin, M., Ormukov, C., & Abdrakhmatov, K. (2012). Inherited strike-slip faults as an origin for basement-cored uplifts: Example of the Kungey and Zailikey ranges, northern Tian Shan. *Tectonics*, 31, TC4026. <https://doi.org/10.1029/2011TC003002>
- Sloan, R. A., Jackson, J. A., McKenzie, D., & Priestley, K. (2011). Earthquake depth distributions in central Asia, and their relations with lithosphere thickness, shortening and extension. *Geophysical Journal International*, 185(1), 1–29. <https://doi.org/10.1111/j.1365-246X.2010.04882.x>
- Smekalin, O. P., Imaev, V. S., Korzhenkov, A. M., & Chipizubov, A. V. (2016). Paleoseismological investigations in the pleistoseismal zone of the 1885 Belovodskoe earthquake, north Tien Shan. *Seismic Instruments*, 52(4), 279–289.
- Smith, B., & Sandwell, D. (2003). Accuracy and resolution of shuttle radar topography mission data. *Geophysical Research Letters*, 30(9), 1467. <https://doi.org/10.1029/2002GL016643>
- Sobel, E. R., Oskin, M. E., Burbank, D. W., & Nikolaichuk, A. (2006). Exhumation of basement-cored uplifts: Example of the Kyrgyz range quantified with apatite fission-track thermochronology. *Tectonics*, 25, TC2008. <https://doi.org/10.1029/2005TC001809>
- Takeuchi, N., Fujita, K., Aizen, V. B., Narama, C., Yokoyama, Y., Okamoto, S., ... Kubota, J. (2014). The disappearance of glaciers in the Tien Shan Mountains in Central Asia at the end of Pleistocene. *Quaternary Science Reviews*, 103, 26–33.
- Tatevossian, R. E. (2007). The Verny, 1887, earthquake in Central Asia: Application of the INQUA scale, based on coseismic environmental effects. *Quaternary International*, 173, 23–29.
- Thompson Jobe, J. A., Li, T., Chen, J., Burbank, D. W., & Bufer, A. (2017). Quaternary tectonic evolution of the Pamir–Tian Shan convergence zone, Northwest China. *Tectonics*, 36. <https://doi.org/10.1002/2017TC004541>
- Thompson, S. C. (2001). Active tectonics in the central Tien Shan, Kyrgyz Republic, (PhD thesis). WA: University of Washington.
- Thompson, S. C., Weldon, R. J., Rubin, C. M., Abdrakhmatov, K., Molnar, P., & Berger, G. W. (2002). Late Quaternary slip rates across the central Tien Shan, Kyrgyzstan, central Asia. *Journal of Geophysical Research*, 107(B9), 2203. <https://doi.org/10.1029/2001JB000596>
- Tibaldi, A., Grazierio, E., Forcella, F., & Gapich, V. H. (1997). Morphotectonic indicators of Holocene faulting in central Tien Shan, Kazakhstan, and geodynamic implications. *Journal of Geodynamics*, 23(1), 23–45.
- Torizin, J., Jentzsch, G., Malischewsky, P., Kley, J., Abakanov, T., & Kurskeev, A. (2009). Rating of seismicity and reconstruction of the fault geometries in northern Tien Shan within the project “Seismic Hazard Assessment for Almaty”. *Journal of Geodynamics*, 48(3–5), 269–278.
- Walker, R., Jackson, J., & Baker, C. (2003). Surface expression of thrust faulting in eastern Iran: Source parameters and surface deformation of the 1978 Tabas and 1968 Ferdows earthquake sequences. *Geophysical Journal International*, 152(3), 749–765.
- Wang, K., & Fialko, Y. (2015). Slip model of the 2015 M_w 7.8 Gorkha (Nepal) earthquake from inversions of ALOS-2 and GPS data. *Geophysical Research Letters*, 42, 7452–7458. <https://doi.org/10.1002/2015GL065201>
- Wells, D. L., & Coppersmith, K. J. (1994). New empirical relationships among magnitude, rupture length, rupture width, rupture area, and surface displacement. *Bulletin of the Seismological Society of America*, 84(4), 974–1002.
- Wesnousky, S. G. (2006). Predicting the endpoints of earthquake ruptures. *Nature*, 444(7117), 358–360.
- Wesnousky, S. G. (2008). Displacement and geometrical characteristics of earthquake surface ruptures: Issues and implications for seismic-hazard analysis and the process of earthquake rupture. *Bulletin of the Seismological Society of America*, 98(4), 1609–1632.
- Wessel, P., & Smith, W. H. (1998). New improved version of generic mapping tools released. *Eos, Transactions American Geophysical Union*, 79(47), 579. <https://doi.org/10.1029/98EO00426>
- Willett, S. D. (1999). Rheological dependence of extension in wedge models of convergent orogens. *Tectonophysics*, 305(4), 419–435.
- Windley, B. F., Allen, M. B., Zhang, C., Zhao, Z. Y., & Wang, G. R. (1990). Paleozoic accretion and Cenozoic redeformation of the Chinese Tien Shan range, central Asia. *Geology*, 18(2), 128–131.
- Zech, R. (2012). A Late Pleistocene glacial chronology from the Kitschi-Kurumdu Valley, Tien Shan (Kyrgyzstan), based on ^{10}Be surface exposure dating. *Quaternary Research*, 77(02), 281–288.
- Zubovich, A. V., Wang, X., Scherba, Y. G., Schelochkov, G. G., Reilinger, R., Reigber, C., ... Beisenbaev, R. T. (2010). GPS velocity field for the Tien Shan and surrounding regions. *Tectonics*, 29, TC6014. <https://doi.org/10.1029/2010TC002772>